

This discussion paper is/has been under review for the journal Atmospheric Chemistry and Physics (ACP). Please refer to the corresponding final paper in ACP if available.

Model simulated trend of surface carbon monoxide for the 2001–2010 decade

J. Yoon and A. Pozzer

Atmospheric Chemistry Department, Max-Planck Institute of Chemistry, P.O. Box 3060,
55020 Mainz, Germany

Received: 6 May 2014 – Accepted: 7 May 2014 – Published: 14 May 2014

Correspondence to: J. Yoon (jongmin.yoon@mpic.de)

Published by Copernicus Publications on behalf of the European Geosciences Union.

Model simulated trend of surface carbon monoxide

J. Yoon and A. Pozzer

[Title Page](#)

[Abstract](#)

[Introduction](#)

[Conclusions](#)

[References](#)

[Tables](#)

[Figures](#)



[Back](#)

[Close](#)

[Full Screen / Esc](#)

[Printer-friendly Version](#)

[Interactive Discussion](#)



Abstract

We present decadal trend estimates of surface carbon monoxide (CO), simulated using the atmospheric chemistry general circulation model ECHAM5/MESSy (EMAC) based on the emission scenarios, Representative Concentration Pathways (RCP) 8.5 for anthropogenic activity and Global Fire Emissions Database (GFED) v3.1 for biomass burning from 2001 through 2010. The spatial distribution of the modelled surface CO is evaluated with monthly Measurements Of Pollution In The Troposphere (MOPITT) thermal infrared product. The global means of correlation coefficient and relative bias for the 2001–2010 are 0.95 and –4.29 %, respectively. We also find a reasonable correlation ($R = 0.78$) between the trends of EMAC surface CO and full 10 year monthly records from ground-based observation (World Data Centre for Greenhouse Gases, WDCGG). Over Western Europe, Eastern USA, and Northern Australia, the significant decreases of EMAC surface CO are estimated at -35.5 ± 5.8 , -59.6 ± 9.1 , and -13.7 ± 9.5 ppbv decade $^{-1}$, respectively, with a 95 % confidence interval. In contrast, the surface CO increases by $+8.9 \pm 4.8$ ppbv decade $^{-1}$ over South Asia. A high correlation ($R = 0.92$) between the significant changes in EMAC-simulated surface CO and total emission flux shows that the significant regional trends are attributed to the changes in primary/direct emissions from both anthropogenic activity and biomass burning. In particular, increasing trends of surface hydroxyl radical (OH) partially contribute to the decreasing trends of surface CO in Western Europe and Eastern USA.

1 Introduction

Medium-lived and unevenly-mixed carbon monoxide (CO) in the atmosphere is a key tracer in atmospheric chemistry and climate change (Novelli et al., 1992; Forster et al., 2007, IPCC AR4; Duncan and Logan, 2008; Gomez-Pelaez et al., 2013). Major sources of atmospheric CO are fossil fuel combustion and biomass burning on the Earth's surface (Wallace and Hobbs, 2006). CO leads to the formation of tropospheric ozone (O_3)

ACPD

14, 12409–12460, 2014

Model simulated trend of surface carbon monoxide

J. Yoon and A. Pozzer

Title Page

Abstract

Introduction

Conclusions

References

Tables

Figures

◀

▶

◀

▶

Back

Close

Full Screen / Esc

Printer-friendly Version

Interactive Discussion



**Model simulated
trend of surface
carbon monoxide**

J. Yoon and A. Pozzer

[Title Page](#)[Abstract](#)[Introduction](#)[Conclusions](#)[References](#)[Tables](#)[Figures](#)[|◀](#)[▶|](#)[◀](#)[▶|](#)[Back](#)[Close](#)[Full Screen / Esc](#)[Printer-friendly Version](#)[Interactive Discussion](#)

and carbon dioxide (CO_2) through photochemical and oxidation reactions (Crutzen and Gidel, 1983; Fishman and Crutzen, 1978; Burrows et al., 1995). It also controls the hydroxyl radical (OH) concentration and distribution in unpolluted and non-forested locations (Levy, 1971; Thompson, 1992; Crutzen, 1974; Logan et al., 1981), which influences the oxidation of most trace gases on the Earth (Khalil and Rasmussen, 1990), such as methane (CH_4) and other pollutants (Lelieveld et al., 2004; Novelli et al., 1992; Thompson and Cicerone, 1986). Finally it contributes to climate change with direct and indirect radiative forcings around 0.024 and 0.2 W m^{-2} , respectively (Forster et al., 2007, IPCC AR4). Monitoring long-term series of surface CO is therefore important for understanding the influence of the direct CO emissions on atmospheric chemistry and indirectly, on climate. Previous studies showed that CO exhibited an increasing trend (worldwide) before the '90s (Khalil and Rasmussen, 1988) and a decreasing trend (Novelli et al., 1994; Law, 1999) thereafter. Duncan et al. (2007) and Duncan and Logan (2008) reported comprehensive results of the global/regional budget of CO and leading causes of its trends and interannual variability from 1988 to 1997. No studies based on the model-simulations are present, which estimate recent changes in global/regional CO since 2000.

Satellite observations allow scientists and researchers to provide the long-term accumulated data of global CO that are suitable for the global trend analysis (Burrows et al., 2011). Representative satellite instruments are Measurements of Pollution in the Troposphere (MOPITT) on NASA's Terra satellite (Drummond and Mand, 1996; Deeter et al., 2003; Worden et al., 2013), Scanning Imaging Absorption Spectrometer for Atmospheric CHartographY (SCIAMACHY) on ESA's Envisat satellite (Buchwitz et al., 2000, 2004, 2005, 2007), Atmospheric Infrared Sounder (AIRS) on NASA's Aqua satellite (Susskind et al., 2003; Warner et al., 2007, 2010), Tropospheric Emission Spectrometer (TES) on NASA's Aura satellite (Luo et al., 2007a, b; Ho et al., 2009; Kopacz et al., 2010), and Infrared Atmospheric Sounding Interferometer (IASI) on EUMETSAT's Metop satellite (Clerbaux et al., 2009; George et al., 2009; Klonicki et al., 2012). However, satellite observations are not a direct sampling method, so it is

impossible to completely eliminate the uncertainty in the CO retrieval (average errors for individual total column CO estimates: $\pm 5\text{--}6\%$ for MOPITT, $\pm 5\%$ for SCIAMACHY, $\pm 10\%$ for AIRS, $\pm 6\text{--}7\%$ for TES, and $\pm 5\text{--}7\%$ for IASI, de Laat et al., 2007; Worden et al., 2013) due to problems in instrument calibration/stability and lack of complementary information (e.g., atmospheric temperature profile, surface pressure/temperature, and cloud content) (Clerbaux et al., 1999; Deeter et al., 2003). In particular, the retrieval algorithm based on climatology has an inevitable uncertainty in trend estimates (Yoon et al., 2013a). The ground-based observations, in contrast, can provide decades-long and highly accurate records using in situ measurement methods, but only for the ground stations available. Therefore, there is a significant limitation to estimate a reliable trend of global and regional surface CO from the study solely based on satellite-retrieved or ground-based data.

In this study, the ECHAM5/MESSy Atmospheric Chemistry (EMAC) model is used to simulate surface CO trends from 2001 to 2010. The anthropogenic emissions are based on the Representative Concentration Pathways (RCP) 8.5 (Rihai et al., 2007) and the biomass burning emissions on the Global Fire Emissions Database (GFED) v3.1 (Giglio et al., 2010; van der Werf et al., 2010). The main objectives of this study are to analyze the long-term trend of global and regional surface CO, simulated using EMAC model, and to compare them to observationally-derived trends. This paper is organized as follows: in Sect. 2, we describe the EMAC model and emission scenarios used for the global surface CO simulations from 2001 to 2010, and the MOPITT and WDCGG observations for the evaluations of spatial distribution and temporal change in the simulated surface CO. In Sect. 3, the model results are spatially and temporally evaluated through comparison with the observational datasets. In Sect. 4, we estimate the regional and global trends in EMAC-simulated surface CO and explore the major causes for the trends by comparing changes in CO direct emissions. In Sect. 5, we investigate the influence of the surface OH change on the surface CO trend and Sect. 6 summarizes and presents our results and conclusions.

Model simulated
trend of surface
carbon monoxide

J. Yoon and A. Pozzer

Title Page

Abstract

Introduction

Conclusions

References

Tables

Figures

◀

▶

◀

▶

Back

Close

Full Screen / Esc

Printer-friendly Version

Interactive Discussion



2 Model, emission scenarios, and observational data

2.1 ECHAM5/MESSy Atmospheric Chemistry (EMAC) model

The EMAC model is a numerical atmospheric chemistry general circulation model (ACGCM) developed for investigating atmospheric processes and their interaction with ocean, land, and human influences (see Jöckel et al., 2010 and publications at <http://www.messy-interface.org/>). It consists of the fifth generation European Centre Hamburg general circulation model (ECHAM5 version 5.3.02) (Roeckner et al., 2006) and the second version of the Modular Earth Submodel System (MESSy2 version 2.42) (Jöckel et al., 2010). The simulation results have been extensively evaluated with surface, aircraft, and satellite observations in many publications, such as Jöckel et al. (2006) and Pozzer et al. (2007, 2009, 2012a, b). In this study, a T63L31 resolution was used, corresponding to a horizontal resolution of approximately 1.875° by 1.875° in latitude and longitude and a vertical resolution of 31 levels from the surface to 10 hPa.

2.2 Emission scenarios, RCP 8.5 and GFED v3.1

Several emission scenarios, e.g. IS92 scenarios (Leggett et al., 1992) and Special Report on Emission Scenarios (SRES) (Nakicenovic et al., 2000), have been broadly used for the research on greenhouse gases, air pollutants, and future climate (e.g. Hogrefe et al., 2004; Jacobson and Streets, 2009). However, since they are the no-climate-policy scenarios, it fails to explore the impact of different climate policies (van Vuuren et al., 2011). The fifth Intergovernmental Panel for Climate Change Assessment Report 5 (IPCC-AR5) gives an account of the concentration of greenhouse gases with respect to atmospheric radiation affected by anthropogenic activities (van Vuuren et al., 2011). The Representative Concentration Pathways (RCPs) were developed by four individual modeling groups (i.e., NIES, IIASA, JGCRI, and PBL) (Riahi et al., 2007; Fujino et al., 2006; Hijioka et al., 2008; Clarke et al., 2007; Smith and Wigley, 2006; Wise et al., 2009; van Vuuren et al., 2006, 2007, 2011). They consist of four emission

[Title Page](#)[Abstract](#)[Introduction](#)[Conclusions](#)[References](#)[Tables](#)[Figures](#)[|◀](#)[▶|](#)[Back](#)[Close](#)[Full Screen / Esc](#)[Printer-friendly Version](#)[Interactive Discussion](#)

scenarios, also called RCP 2.6, 4.5, 6.0, and 8.5 representing the radiative forcing of anthropogenic activity from 2.6 to 8.5 W m^{-2} in 2100, which depend on the mitigation or emission scenarios (van Vuuren et al., 2011). Among them, the emission RCP 8.5 is used in this study to investigate the influence of anthropogenic activity on the change in surface CO from 2001 to 2010. It assumes that the emissions in greenhouse gases continue to increases till post-2100 and their concentrations are stabilized post-2200 (Riahi et al., 2007; van Vuuren et al., 2011; Meinshausen et al., 2011). The RCP 8.5 has been tested in Granier et al. (2011), which showed that it is a “reasonable” choice for anthropogenic emissions after the year 2000. Figure 1a shows the total mean of monthly emission flux of RCP 8.5 from 2001 and 2010. It illustrates that the high CO emissions due to anthropogenic activities are located in highly-populated regions or the largest urban agglomerations (aka megacities).

Fire is a significant emission source of several trace gases and aerosols, including atmospheric CO (Andreae and Merlet, 2001; Giglio et al., 2010). To consider the influence of CO emission from biomass burning, the Global Fire Emissions Database (GFED) v3.1 is used in this study. It is based on global fire emissions from deforestation, savanna, forest, agricultural and peat fires (van der Werf et al., 2010). The version 3 is updated using the combination of the long-term time series of improved satellite-derived data (e.g. burned area, fire activity, and plant productivity from MODIS, Tropical Rainfall Measuring Mission (TRMM), Visible and Infrared Scanner (VIRS), Along-Track Scanning Radiometer (ATSR), and Advanced Very High Resolution Radiometer (AVHRR)) and model-estimated data (fuel loads and combustion completeness using Carnegie-Ames-Stanford-Approach (CASA) biogeochemical model) from 1997 to 2009 (van der Werf et al., 2010). Figure 1b shows the global mean distribution of monthly GFED v3.1 surface CO emissions from 2001 to 2010, and shows that fire activity in/around tropical rainforests leads to large CO emissions. Direct CO emissions from anthropogenic activity and biomass burning represent around 50 % of the total CO budget (Granier et al., 1999; Duncan et al., 2007; Bergamaschi et al., 2000).

Model simulated trend of surface carbon monoxide

J. Yoon and A. Pozzer

[Title Page](#)[Abstract](#)[Introduction](#)[Conclusions](#)[References](#)[Tables](#)[Figures](#)[|◀](#)[▶|](#)[◀](#)[▶](#)[Back](#)[Close](#)[Full Screen / Esc](#)[Printer-friendly Version](#)[Interactive Discussion](#)

A simulation with constant emission (hereafter, called *CE* scenario) is performed to assess only the possible influence of the meteorological transports on the surface CO trend as shown in Fig. 2a. Emissions in the model simulation CE are kept equal to the year 2000 of RCP 8.5 and GFED v3.1 for all 10 years of the simulation (2001–2010). In addition to the simulation CE, the combination of RCP 8.5 and GFED v3.1 (hereafter, called *RG* scenario) in Fig. 2b is used for simulating a realistic surface CO concentration. It should be noted that in the RCP 8.5, CO emission does slightly decrease (globally) from the beginning of the 21st century (Butler et al., 2012). Finally, chemistry and transport are fully decoupled, so that both simulations have binary identical meteorology (i.e. transport). Additionally, the model has been weakly nudged towards analysis data of the European Centre for Medium-Range Weather Forecast (ECMWF) (Jeuken et al., 1996) up to 100 hPa to obtain realistic model dynamics.

2.3 MOPITT Version 5 Level 3 thermal infrared CO

The Measurements of Pollution in the Troposphere (MOPITT) instrument, launched on board the EOS-Terra spacecraft in 1999, has been providing continuous global products of tropospheric CO (Deeter et al., 2003). The global MOPITT retrieved CO data with high accuracy (expected precisions: 10 %) has been applied to various researches on its sources, transports, and sinks (e.g., publications at <http://www.acd.ucar.edu/mopitt/publications.shtml>). In this study, the MOPITT Version 5 (V5) Level 3 (L3) thermal infrared (TIR) surface CO products in daytime are used since they have been improved in the retrieval sensitivity and accuracy for the lower tropospheric CO (Clerbaux et al., 2009; Worden et al., 2010, 2013; Deeter et al., 2007, 2011, 2012, 2013). The grey line-shaded regions depicted in Fig. 3 and listed in Table 1, including the globe, Northern, and Southern Hemispheres, are selected for the spatial evaluation and trend estimates. These regions are important to monitor the surface CO released from anthropogenic and fire activities (see Fig. 1).

[Title Page](#)

[Abstract](#)

[Introduction](#)

[Conclusions](#)

[References](#)

[Tables](#)

[Figures](#)

◀

▶

[Back](#)

[Close](#)

[Full Screen / Esc](#)

[Printer-friendly Version](#)

[Interactive Discussion](#)



2.4 WDCGG surface CO

The World Data Centre for Greenhouse Gases (WDCGG) under the World Meteorological Organization/Global Atmosphere Watch (WMO/GAW; http://www.wmo.int/pages/prog/arep/gaw/gaw_home_en.html) was established in 1990 by the Japan Meteorological Agency (JMA) to assist in more reliable monitoring and analysing of greenhouse (CO_2 , CH_4 , CFCs, N_2O , surface ozone, etc.) and related gases (CO, NO_x , SO_2 , VOC, etc.) (<http://ds.data.jma.go.jp/gmd/wdcgg/introduction.html>). The WDCGG-archived CO data are categorized according to the observation platforms or analytical methods (see more details in GAW Report No. 188, WMO, 2009). The full 10 year monthly records of air sampling observations at the stationary platforms (shown as green dots in Fig. 3) were used to evaluate the temporal trend of EMAC-simulated surface CO. Detailed information about the station's geolocations, measurement methods, and contributors are listed in Table 2.

3 Evaluation of EMAC-simulated surface CO

15 3.1 Evaluation of spatial distribution using MOPITT V5 L3 TIR surface CO

Using mostly passive remote sensing instruments (including MOPITT), it is quite challenging to retrieve tropospheric CO profiles because of a significant dependence on atmospheric temperature profile, surface pressure, and surface temperature in the retrieval algorithms (Deeter et al., 2003). In particular, without proper additional information, it is difficult to avoid the systematic error in the retrieved profiles from the algorithm developed that is based on climatology (i.e. a priori CO profiles) (Eskes and Boersma, 2003). This is why the averaging kernels, reflecting the relation between the retrieved and true profiles (Pan et al., 1998; Rodgers, 2000; Deeter et al., 2003), are important for a proper comparison between satellite-retrieved and model-simulated profiles (Rodgers, 2000; Rodger and Connor, 2003; Eskes and Boersma, 2003). The

Title Page	
Abstract	Introduction
Conclusions	References
Tables	Figures
◀	▶
◀	▶
Back	Close
Full Screen / Esc	
Printer-friendly Version	
Interactive Discussion	



EMAC-simulated surface CO can be transformed into a comparable quantity (so called pseudo-retrieval, $\hat{x}_{\text{EMAC}}^{\text{surface}}$), to the MOPITT-retrieved surface CO as follows:

$$\hat{x}_{\text{EMAC}}^{\text{surface}} \equiv \hat{x}_{\text{MOPITT}}^{\text{surface}} + A_{\text{MOPITT}}^{\text{surface}} (x_{\text{EMAC}} - \hat{x}_{\text{MOPITT}}) \quad (1)$$

where $\hat{x}_{\text{MOPITT}}^{\text{surface}}$, $A_{\text{MOPITT}}^{\text{surface}}$, \hat{x}_{MOPITT} , and x_{EMAC} , and represent the MOPITT surface a priori CO, surface averaging kernels matrix, a priori CO profiles, and EMAC-simulated CO profiles from surface to 100 hPa, respectively.

Figure 4 presents the global distributions of the MOPITT surface CO and the pseudo-retrievals based on the EMAC results (CE and RG). Both pseudo-retrievals are similar to the distribution of the remote-sensed MOPITT surface CO: the high concentration of surface CO emanating from the source regions over the Eastern USA, Western Europe, Central Africa, and South/East Asia is due to the combustion of fossil fuels and biomass burning (Wallace and Hobbs, 2006; Worden et al., 2013), while the transported CO by the atmospheric circulation can be detected over neighbouring areas. To further analyse a spatial correlation between the global distributions of MOPITT-retrieved and EMAC-simulated surface CO, we compared them directly. The EMAC-simulated surface CO based on the realistic RG scenario obviously shows better agreement with MOPITT surface CO; for example, as in December 2008 (see Fig. 5) (i.e., the spatial correlation coefficient (R) and the slope of the linear best-fit line (A) are 0.97 and 1.072 ± 0.003 , respectively) than the surface CO based on the CE scenario ($R = 0.92$ and $A = 0.771 \pm 0.003$).

The Taylor diagrams (Taylor, 2001; Forster et al., 2007; Meehl et al., 2007) in Fig. 6 graphically resume the spatial correlation coefficient (R), normalized standard deviation (STD), and normalized centred root-mean-square (RMS) difference for the different regions (see Fig. 3 and Table 1) and for the globe. These statistical quantities are listed in Table 3. In Fig. 6, the more closely the simulated pattern is located to the “Obs.” on x-axis, the more closely it matches up with the observed spatial pattern. Additionally, the relative bias (B) is included in Fig. 6, allowing a more effective comparison

Title Page	
Abstract	Introduction
Conclusions	References
Tables	Figures
	
	
Back	Close
Full Screen / Esc	
Printer-friendly Version	
Interactive Discussion	



between the spatial patterns of the monthly EMAC-simulated and MOPITT-observed CO. As mentioned already and shown again in Fig. 6b, the RG simulation results are more consistent with the MOPITT observations (i.e. in most regions, R is greater than about 0.9, less than about ± 0.25 of normalized STD, less than about 0.5 of normalized centred RMS difference, and less than about $\pm 10\%$ of B) than the one based on CE scenario in Fig. 6a. Therefore, we can conclude that the simulation RG agrees well with the MOPITT-observed surface CO in the spatial distribution. Rather poor agreement at the Pacific Region (PAR) can be explained by the biases in the MOPITT CO surface retrievals at cleaner locations, such as over the Pacific Ocean (Emmons et al., 2004) and the failings to consider significant influences of natural sources (e.g. effects of the El Niño on tropospheric CO, Chandra et al., 2009) in the EMAC model.

3.2 Evaluation of temporal change using WDCGG surface CO

In this section, the WDCGG surface CO observations at the stationary sites (see Fig. 3 and Table 2) are used to evaluate the temporal changes of EMAC simulations. We applied the monthly time series (Y_t) of EMAC-simulated and WDCGG-archived data to a linear trend model. The following form of a typical linear model has been adopted in various studies (Zhao et al., 2008; Hsu et al., 2012; de Meij et al., 2012; Yoon et al., 2011, 2012, 2013a, b) for estimating climatological changes in the atmospheric system (Weatherhead et al., 1998, 2002).

$$20 \quad Y_t = \mu + \omega X_t + S_t + N_t \quad (2)$$

where μ , ω , and X_t denote the constant, the magnitude of the trend per year, and the time index term ($t/12$), respectively. S_t is a seasonal component fitted using Fourier analysis as follows:

$$25 \quad S_t = \sum_{j=1}^4 [\beta_{1,j} \sin(2\pi jt/12) + \beta_{2,j} \cos(2\pi jt/12)]. \quad (3)$$

[Title Page](#)[Abstract](#)[Introduction](#)[Conclusions](#)[References](#)[Tables](#)[Figures](#)[◀](#)[▶](#)[Back](#)[Close](#)[Full Screen / Esc](#)[Printer-friendly Version](#)[Interactive Discussion](#)

N_t is the unexplained noise term, which is often assumed to be autocorrelated with one time lag (Weatherhead et al., 1998, 2002) as follows:

$$N_t = \varphi N_{t-1} + \varepsilon_t \quad (4)$$

- 5 where φ is the autocorrelation coefficient ($-1 < \varphi < 1$) and ε_t is an independent random variable. If $\hat{\omega}$ denotes the trend estimate in Eq. (2), determined by minimizing the chi-square error statistic, the standard deviation ($\sigma_{\hat{\omega}}$) of the trend estimate can be quite accurately approximated as follows:

$$\sigma_{\hat{\omega}} \approx \frac{\sigma_{\varepsilon}}{(1 - \varphi)} \frac{1}{n^{3/2}} = \frac{\sigma_N}{n^{3/2}} \sqrt{\frac{1 + \varphi}{1 - \varphi}} \quad (5)$$

10 where σ_{ε} , σ_N , and n denote the standard deviation of ε and N , and the number of years, respectively. In this study, we define $\hat{\omega}$ as a statistically significant trend at a 95 % confidence level when $|\hat{\omega}/\sigma_{\hat{\omega}}|$ is larger than two (Tiao et al., 1990; Weatherhead et al., 1998). This method is strictly applied to the full 10 year monthly records to minimize 15 statistical biases from data inconsistencies in the trend estimates. In the same manner, the trends are derived from the EMAC-simulated surface CO data based on CE and RG scenarios at the closest grid to the WDCGG stations (see Table 2).

20 The trends of EMAC-simulated surface CO based on the RG scenario show better agreement and higher correlation (i.e., the correlation coefficient (R) and the slope of linear best-fit line (A) are 0.60 and 0.93 ± 0.40 in Fig. 7b) with the WDCGG trend than the ones based on the CE scenario ($R = -0.32$ and $A = -0.06 \pm 0.06$ in Fig. 7a). The difference is more clearly shown in the comparison between only significant trends 25 ($R = 0.94$ and $A = 0.20 \pm 0.11$ in Fig. 7a, and $R = 0.70$ and $A = 1.02 \pm 0.93$ in Fig. 7b). The specific values of trend estimates and statistical quantities are summarized in Table 4. At some stations (i.e. Cape Point, Key Biscayne, Niwot Ridge, Park Falls, Point Arena, Rigi, Sede Boker, and Tae-ahn Peninsula) influenced by local pollution or its transports, the trends of EMAC-simulated surface CO based on the RG scenario

Model simulated trend of surface carbon monoxide

J. Yoon and A. Pozzer

Title Page

Abstract

Introduction

Conclusions

References

Tables

Figures

◀

▶

◀

▶

Back

Close

Full Screen / Esc

Printer-friendly Version

Interactive Discussion



are considerably different to the WDCGG trends. It is attributed to the WDCGG flask sampling method to minimize the contamination from local pollution (Haas-Laursea and Hartley, 1997) and the rather low resolution of the EMAC model grid, which cannot discriminate the local sources (Pozzer et al., 2007). Therefore, for such stations, we have not used the closest grid of EMAC-simulated surface CO to the WDCGG stations, but a model grid-box to the upwind direction as suggested in Pozzer et al. (2007). Again, Fig. 8 presents the comparison between the trends of EMAC-simulated surface CO based on the RG scenario and WDCGG-archived surface CO. A better correlation coefficient and slope of linear best-fit line are obtained ($R = 0.78$ and $A = 0.94 \pm 0.25$). Therefore, we can conclude that the long-term simulations based on the RG scenario provide statistically reliable trend estimates of global surface CO.

4 Global, latitudinal, and regional trend estimates of EMAC-simulated surface CO

4.1 Global and latitudinal scales

After the Mt. Pinatubo eruption on June 1991, the global surface CO from 1991 to 2001 decreased by $-0.52 \text{ ppb yr}^{-1}$ (Novelli et al., 2003). It is attributed to the aftereffect of the eruption (Dlugokencky et al., 1996) and the subsequent increase in surface atmospheric OH (Bekki et al., 1994). Novelli et al. (2003) reported the decrease of CO (-1.4 ppb yr^{-1}) in the northern extra-tropics caused by the decrease in anthropogenic emissions in the Northern Hemisphere from 1991 to 2001, but there was no significant trend in the Southern Hemisphere. Similarly, Duncan and Logan (2008) found that the decrease in European emissions leads to a decreasing trend ($-0.85 \% \text{ yr}^{-1}$) in northern extra-tropics from 1988 to 1997. Worden et al. (2013) showed that the entire CO column still has a small negative trend in recent years (below $1 \% \text{ yr}^{-1}$), from 2000 through 2011, with a strong decrease of CO over the US, Europe and China, although it is not clear what is behind such trends.

Model simulated trend of surface carbon monoxide

J. Yoon and A. Pozzer

[Title Page](#)

[Abstract](#)

[Introduction](#)

[Conclusions](#)

[References](#)

[Tables](#)

[Figures](#)

◀

▶

◀

▶

[Back](#)

[Close](#)

[Full Screen / Esc](#)

[Printer-friendly Version](#)

[Interactive Discussion](#)



Model simulated trend of surface carbon monoxide

J. Yoon and A. Pozzer

[Title Page](#)[Abstract](#)[Introduction](#)[Conclusions](#)[References](#)[Tables](#)[Figures](#)[|◀](#)[▶|](#)[Back](#)[Close](#)[Full Screen / Esc](#)[Printer-friendly Version](#)[Interactive Discussion](#)

Figure 9 presents the global trend of EMAC-simulated surface CO based on the CE and RG scenarios. The trends estimated in simulation CE could be purely attributed to dynamical changes as emissions and long-lived species are constant throughout the entire simulation. These trends (Fig. 9a) are statistically significant in the Southern Hemisphere and their magnitudes are relatively small. These are nevertheless not significant when changing emissions are included (simulation RG, Fig. 9b). In the realistic simulation RG (Fig. 9b), generally decreasing trends are predominant, in particular over Europe and the Eastern USA as a result of strict environmental regulation (Streets et al., 2003; Yoon et al., 2011, 2012, 2013b; Hilboll et al., 2013), and Southeast Asia due to less fire activity (Giglio et al., 2010). They are consistent with the WDCGG-archived trends (see Sect. 3.2) as well as the decreasing trends in total CO columns retrieved from MOPITT and AIRS satellite instruments (MOPITT: $-1.44 \pm 0.44\% \text{ yr}^{-1}$ for Europe and $-1.42 \pm 0.40\% \text{ yr}^{-1}$ for the Eastern USA, AIRS: $-1.00 \pm 0.66\% \text{ yr}^{-1}$ and $-0.96 \pm 0.36\% \text{ yr}^{-1}$, with $\pm 2\sigma$ errors, respectively) (Worden et al., 2013). In contrast, upward trends are estimated over the quickly developing countries and the forested regions (i.e., around South Asia, East China, Central South America, Central/Southern Africa). They can be attributed to the increases of anthropogenic and fire activities (Burrows et al., 1995; Bovensmann et al., 1999; Richter et al., 2005; Giglio et al., 2010). More significant signals in the trend estimates are found in the Northern Hemisphere than Southern Hemisphere. These differences are clearly shown in Fig. 10, which depicts the latitudinal means and corresponding trends of the EMAC-simulated surface CO from 90° S to 90° N at 1.875° intervals. The mixing ratio of surface CO is definitely higher in the Northern Hemisphere where about 90 % of the human population resides. Finally, in simulation CE (Fig. 10a), almost no change in the EMAC-simulated surface CO is estimated over all latitudinal ranges. Contrariwise, in simulation RG, the surface CO shows a significant decreasing trend (Fig. 10b), especially between 30° N to 60° N the mean trend with $\pm 2\sigma$ errors is $-19.46 \pm 11.79 \text{ ppbv decade}^{-1}$. Novelli et al. (2003) and Duncan and Logan (2008) also reported a similar tendency in northern extra-tropics influenced by the decrease in anthropogenic emissions in the North-

ern Hemisphere for the decade 1988–2001. At lower latitudes (i.e. less than 30° N), the same simulation shows no significant trends. These latitudinal tendencies generally show good agreement with the significant trends of WDCGG-archived data except the one at the stations Hegyhatsal and Payerne located in Eastern Europe where the downward trend (i.e. -52.26 ± 31.63 and -52.76 ± 22.21 ppbv decade $^{-1}$, respectively) is relatively high compared to the same latitudinal trends (see Table 4).

4.2 Regional scale

The sources of tropospheric CO are in situ oxidations and direct emissions: primarily oxidation of CH₄ (~ 800 Tg(CO) yr $^{-1}$) and emissions from biomass burning (~ 700 Tg(CO) yr $^{-1}$) and fossil/domestic fuel (~ 650 Tg(CO) yr $^{-1}$) (Bergamaschi et al., 2000; WMO, 1999; IPCC, 1996; Ehhalt et al., 2001). In particular, only the direct emissions account for around 50 % of the total CO budget (Ehhalt et al., 2001). In this section, we estimate the surface CO trends by the region and compare them with the changes in the direct emissions.

Figure 11 shows the regional trends of EMAC-simulated surface CO for the selected regions (see Table 1 and Fig. 3), and Fig. 12 shows the corresponding changes in the emissions from anthropogenic activity and the biomass burning dataset (i.e. RCP 8.5 and GFED v3.1).

The Pacific Region (PAR) is a remote area over open oceans and is the focus of many studies on climate change (e.g. Trenberth et al., 2002; Latif and Keenlyside, 2009; Rieder et al., 2013) since it is sensitive to El Niño and La Niña-Southern Oscillation (Rasmusson and Carpenter, 1982). Although PAR is almost not influenced by human activity, shipping transport in this region still plays a role on the CO concentration. The significant trend of EMAC surface CO is estimated (-5.8 ± 5.5 ppbv decade $^{-1}$) and consistent with significant trend of monthly anthropogenic emission (-0.007 ± 0.003 MtCO decade $^{-1}$).

The Eastern USA (EUSA) and Western Europe (WE) are highly industrialized countries/regions (Zhang et al., 2012; Yoon et al., 2011), where anthropogenic CO

[Title Page](#)[Abstract](#)[Introduction](#)[Conclusions](#)[References](#)[Tables](#)[Figures](#)[|◀](#)[▶|](#)[Back](#)[Close](#)[Full Screen / Esc](#)[Printer-friendly Version](#)[Interactive Discussion](#)

emissions are predominant (see Fig. 1a). An occasional influence from biomass burning is found, as shown in Fig. 12. As a result of environmental regulations over these regions during past decades (Streets et al., 2003; Yoon et al., 2011, 2012, 2013b), the decreasing trends of atmospheric aerosol and short-lived trace gases have been reported in many studies (e.g. Smith et al., 2001; Streets et al., 2006; Richter et al., 2005; Hilboll et al., 2013). The dramatic decreases of EMAC surface CO are estimated ($-59.6 \pm 9.1 \text{ ppbv decade}^{-1}$ for EUSA and $-35.5 \pm 5.8 \text{ ppbv decade}^{-1}$ for WE) and are compatible (see Fig. 12) with the significant change in monthly emissions ($-2.101 \pm 0.328 \text{ MtCO decade}^{-1}$ for EUSA and $-0.856 \pm 0.036 \text{ MtCO decade}^{-1}$ for WE). These results are comparable to Worden et al. (2013) and Angelbratt et al. (2011), which derived the downward trends in MO-PITT total CO column ($(-3.14 \pm 0.88) \times 10^{16} \text{ molecules cm}^{-2} \text{ yr}^{-1}$ for Eastern USA and $(-3.03 \pm 0.92) \times 10^{16} \text{ molecules cm}^{-2} \text{ yr}^{-1}$ for Europe) and solar FTIR partial CO column (i.e. $\sim 0\text{--}15 \text{ km}$) ($-0.45 \pm 0.16 \% \text{ yr}^{-1}$, $-1.00 \pm 0.24 \% \text{ yr}^{-1}$, $-0.62 \pm 0.19 \% \text{ yr}^{-1}$ and $-0.61 \pm 0.16 \% \text{ yr}^{-1}$ at the ground-based stations Jungfraujoch, Zugspitze, Harestua, and Kiruna over Europe).

Central South America, Central/Southern Africa, SouthEast Asia, and Northern Australia (i.e. CSA, CAF, SAF, SEA, and NA) are representative for the tropical rainforests (Ahlm et al., 2009; Eltahir and Bras, 1996; Li and Fu, 2004; Nepstad et al., 1999; Held et al., 2005; Chung and Ramanathan, 2006; Facchini et al., 2000; McFiggans et al., 2005, 2006). Over these regions, a large amount of surface CO has been emitted by biomass burning (see Figs. 1b and 12) through deforestation caused by land use, subsistence agriculture, and spontaneous combustion in warm and dry seasons (Reeves et al., 2010; Johnson et al., 2008; Kirby et al., 2006; Davidson and Artaxo, 2004). Insignificant trends in EMAC-simulated surface CO are estimated over these regions ($+30.0 \pm 53.4 \text{ ppbv decade}^{-1}$ for CSA, $+2.2 \pm 7.4 \text{ ppbv decade}^{-1}$ for CAF, $+7.2 \pm 10.5 \text{ ppbv decade}^{-1}$ for SAF, and $-21.3 \pm 39.1 \text{ ppbv decade}^{-1}$ for SEA) except in NA ($-13.7 \pm 9.5 \text{ ppbv decade}^{-1}$) because of the strong interannual variability of biomass burning emission as shown in Fig. 12.

Model simulated trend of surface carbon monoxide

J. Yoon and A. Pozzer

[Title Page](#)

[Abstract](#)

[Introduction](#)

[Conclusions](#)

[References](#)

[Tables](#)

[Figures](#)

◀

▶

◀

▶

[Back](#)

[Close](#)

[Full Screen / Esc](#)

[Printer-friendly Version](#)

[Interactive Discussion](#)



China and India are highly-populated and developing countries occupying about 36.5 % of the world population in 2013 (http://en.wikipedia.org/wiki/List_of_countries_by_population) and 14.1 % of world GDP in 2012 (World Bank Data, <http://data.worldbank.org/>). As a consequence, large amounts of anthropogenic pollutants (e.g. aerosols, nitrogen dioxide, sulfur dioxide, and surface ozone) that lead to environmental and health problems are emitted into the atmosphere (Ohara et al., 2007; Pozzer et al., 2012a, 2012b; Lelieveld et al., 2013). The long-term change in these pollutants has been a key issue in many studies (e.g. Yoon et al., 2012, 2013b; Richter et al., 2005; Hilboll et al., 2013; Lu et al., 2010; Xu et al., 2008). The increases of EMAC surface CO are estimated in both regions ($+8.9 \pm 4.8 \text{ ppbv decade}^{-1}$ for SA and $+9.1 \pm 9.7 \text{ ppbv decade}^{-1}$ for EC). In the case of EC, since the trend is not statistically significant and is opposite to the decreasing trend in the emission ($-0.116 \pm 0.094 \text{ MtCO decade}^{-1}$), it is influenced by the changes in transports or secondary chemical production (Tohjima et al., 2014; Angelbratt et al., 2011).

On a global scale, the simulation RG shows a significant trend only in the NH ($-13.5 \pm 11.1 \text{ ppbv decade}^{-1}$ for the NH, $-0.8 \pm 6.7 \text{ ppbv decade}^{-1}$ for the SH, and $-7.2 \pm 7.8 \text{ ppbv decade}^{-1}$ for the GL). Notably, the evident change in NH CO is attributed to the significant change in emissions ($-6.940 \pm 3.805 \text{ MtCO decade}^{-1}$). Figure 13 clearly shows a high correlation between the trends in EMAC-simulated surface CO and total emission flux ($R = 0.88$ between all trends and $R = 0.92$ between significant trends). Since the trends of WDCGG-archived surface CO are highly correlated with the EMAC-simulated trends as shown in Fig. 8, we can confirm that the changes in surface CO over the past decade are mostly due to changes in the emissions.

5 Influence of surface OH trend

Hydroxyl radical (OH) is the main oxidant of many trace gases and therefore one of the most important species in the atmospheric chemistry (Lawrence et al., 2001; Wallace and Hobbs, 2006). CO removal from the troposphere is almost exclusively by reaction

Model simulated trend of surface carbon monoxide

J. Yoon and A. Pozzer

[Title Page](#)

[Abstract](#)

[Introduction](#)

[Conclusions](#)

[References](#)

[Tables](#)

[Figures](#)

[|◀](#)

[▶|](#)

[◀](#)

[▶](#)

[Back](#)

[Close](#)

[Full Screen / Esc](#)

[Printer-friendly Version](#)

[Interactive Discussion](#)



Model simulated trend of surface carbon monoxide

J. Yoon and A. Pozzer

[Title Page](#)

[Abstract](#)

[Introduction](#)

[Conclusions](#)

[References](#)

[Tables](#)

[Figures](#)

[◀](#)

[▶](#)

[◀](#)

[▶](#)

[Back](#)

[Close](#)

[Full Screen / Esc](#)

[Printer-friendly Version](#)

[Interactive Discussion](#)



6 Summary and conclusion

The global and regional changes in surface CO have been estimated using the EMAC model from 2001 to 2010. The spatial distributions and temporal changes in the EMAC-simulated surface CO based on CE and RG scenarios have been extensively evaluated with results derived from MOPITT-retrieved and WDCGG-archived data. We have shown that the spatial distribution and temporal change of EMAC-simulated surface CO based on the RG scenario are consistent with the observational datasets. Significant trends of the EMAC surface CO have been found in the Northern Hemisphere (confirming the decreasing trends already reported in the northern extra-tropics in the decade 1988–2001), in particular, a decreasing trend over the Eastern USA, Western Europe, and an increasing trend over South Asia, mostly due to the changes of anthropogenic emission. Additionally, the increasing trend of surface OH contributes to the decrease of surface CO in these regions. In contrast, over the regions influenced by biomass burning (i.e. Central South America, Central Africa, Southern Africa, and Southeast Asia), no significant trend has been detected because of a high interannual variability of fire activity.

Acknowledgements. The authors would like to thank the NASA Langley Research Center (Atmospheric Science Data Center, <https://eosweb.larc.nasa.gov/>) and World Data Centre for Greenhouse Gases (WDCGG, <http://ds.data.jma.go.jp/gmd/wdcgg/>) for providing the MOPITT Version 5 TIR Level 3 products and monthly WDCGG-archived surface CO data used in the study. We gratefully acknowledge the efforts of the EMAC development team to develop and make available the EMAC modelling system.

The service charges for this open access publication
have been covered by the Max Planck Society.

Title Page

Abstract

Introduction

Conclusions

References

Tables

Figures

◀

▶

Back

Close

Full Screen / Esc

Printer-friendly Version

Interactive Discussion



References

- Ahlm, L., Nilsson, E. D., Krejci, R., Mårtensson, E. M., Vogt, M., and Artaxo, P.: Aerosol number fluxes over the Amazon rain forest during the wet season, *Atmos. Chem. Phys.*, 9, 9381–9400, doi:10.5194/acp-9-9381-2009, 2009.
- 5 Andreae, M. O. and Merlet, P.: Emission of trace gases and aerosols from biomass burning, *Global Biogeochem. Cy.*, 15, 955–966, doi:10.1029/2000GB001382, 2001.
- Angelbratt, J., Mellqvist, J., Simpson, D., Jonson, J. E., Blumenstock, T., Borsdorff, T., Duchatelet, P., Forster, F., Hase, F., Mahieu, E., De Mazière, M., Notholt, J., Petersen, A. K., Raffalski, U., Servais, C., Sussmann, R., Warneke, T., and Vigouroux, C.: Carbon monoxide (CO) and ethane (C_2H_6) trends from ground-based solar FTIR measurements at six European stations, comparison and sensitivity analysis with the EMEP model, *Atmos. Chem. Phys.*, 11, 9253–9269, doi:10.5194/acp-11-9253-2011, 2011.
- Bekki, S., Law, K. S., and Pyle, J. A.: Effect of ozone depletion on atmospheric methane and CO concentrations, *Nature*, 371, 595–597, doi:10.1038/371595a0, 1994.
- 10 Bergamaschi, P., Hein, R., Heimann, M., Crutzen, P. J.: Inverse modeling of the global CO cycle: 1. Inversion of CO mixing ratios, *J. Geophys. Res.-Atmos.*, 105, D2, 1909–1927, doi:10.1029/1999JD9000818, 2000.
- Bovensmann, H., Burrows, J. P., Buchwitz, M., Frerick, J., Noël, S., Rozanov, V. V., Chance, K. V., and Goede, A. P. H.: SCIAMACHY – mission objectives and measurement modes, *J. Atmos. Sci.*, 56, 127–150, doi:10.1175/1520-0469(1999)056<0127:SMOAMM>2.0.CO;2, 1999.
- 20 Buchwitz, M., Rozanov, V. V., and Burrows, J. P.: A near-infrared optimized DOAS method for the fast global retrieval of atmospheric CH_4 , CO, CO_2 , H_2O , and N_2O total column amounts from SCIAMACHY Envisat-1 nadir radiances, *J. Geophys. Res.-Atmos.*, 105, 15231–15245, 2000.
- Buchwitz, M., de Beek, R., Bramstedt, K., Noël, S., Bovensmann, H., and Burrows, J. P.: Global carbon monoxide as retrieved from SCIAMACHY by WFM-DOAS, *Atmos. Chem. Phys.*, 4, 1945–1960, doi:10.5194/acp-4-1945-2004, 2004.
- 25 Buchwitz, M., de Beek, R., Noël, S., Burrows, J. P., Bovensmann, H., Bremer, H., Bergamaschi, P., Körner, S., and Heimann, M.: Carbon monoxide, methane and carbon dioxide columns retrieved from SCIAMACHY by WFM-DOAS: year 2003 initial data set, *Atmos. Chem. Phys.*, 5, 3313–3329, doi:10.5194/acp-5-3313-2005, 2005.

Model simulated trend of surface carbon monoxide

J. Yoon and A. Pozzer

Title Page

Abstract

Introduction

Conclusions

References

Tables

Figures

◀

▶

Back

Close

Full Screen / Esc

Printer-friendly Version

Interactive Discussion



- Buchwitz, M., Khlystova, I., Bovensmann, H., and Burrows, J. P.: Three years of global carbon monoxide from SCIAMACHY: comparison with MOPITT and first results related to the detection of enhanced CO over cities, *Atmos. Chem. Phys.*, 7, 2399–2411, doi:10.5194/acp-7-2399-2007, 2007.
- 5 Burrows, J. P., Hözle, E., Goede, A. P. H., Visser, H., and Fricke, W.: SCIAMACHY – Scanning Imaging Absorption Spectrometer for Atmospheric Chartography, *Acta Astronaut.*, 35, 445–451, 1995.
- 10 Burrows, J. P., Goede, A. P. H., Muller, C., and Bovensmann, H.: SCIAMACHY – the need for atmospheric research from space, in: SCIAMACHY – Exploring the Changing Earth's Atmosphere, edited by: Gottwald, M., and Bovensmann, H., Springer Science+Business Media B. V., Dordrecht, Netherlands, 1–17, doi:10.1007/978-90-481-9896-2_1, 2011.
- 15 Butler, T. M., Stock, Z. S., Russo, M. R., Denier van der Gon, H. A. C., and Lawrence, M. G.: Megacity ozone air quality under four alternative future scenarios, *Atmos. Chem. Phys.*, 12, 4413–4428, doi:10.5194/acp-12-4413-2012, 2012.
- 20 Chandra, S., Ziemke, J. R., Duncan, B. N., Diehl, T. L., Livesey, N. J., and Froidevaux, L.: Effects of the 2006 El Niño on tropospheric ozone and carbon monoxide: implications for dynamics and biomass burning, *Atmos. Chem. Phys.*, 9, 4239–4249, doi:10.5194/acp-9-4239-2009, 2009.
- 25 Chung, C. E. and Ramanathan, V.: Weakening of North Indian SST Gradients and the Monsoon Rainfall in India and the Sahel, *J. Climate*, 19, 2036–2045, doi:10.1175/JCLI3820.1, 2006.
- Clarke, L., Edmonds, J., Jacoby, H., Pitcher, H., Reilly, J., and Richels, R.: Scenarios of Greenhouse Gas Emissions and Atmospheric Concentrations. Sub-report 2.1A of Synthesis and Assessment Product 2.1, USGCRP Department of Energy, Office of Biological & Environ. Res., Washington DC, USA, 154 pp., 2007.
- 30 Clerbaux, C., Hadji-Lazaro, J., Payan, S., Camy-Peyret, C., and Mégie, G.: Retrieval of CO columns from IMG/ADEOS spectra, *IEEE T. Geosci. Remote*, 37, 3, 1657–1661, 1999.
- Clerbaux, C., Boynard, A., Clarisse, L., George, M., Hadji-Lazaro, J., Herbin, H., Hurtmans, D., Pommier, M., Razavi, A., Turquety, S., Wespes, C., and Coheur, P.-F.: Monitoring of atmospheric composition using the thermal infrared IASI/MetOp sounder, *Atmos. Chem. Phys.*, 9, 6041–6054, doi:10.5194/acp-9-6041-2009, 2009.
- 35 Crutzen, P. J.: Photochemical reactions initiated by and influencing ozone in unpolluted tropospheric air, *Tellus*, 26, 47–57, 1974.

Model simulated trend of surface carbon monoxide

J. Yoon and A. Pozzer

[Title Page](#)

[Abstract](#)

[Introduction](#)

[Conclusions](#)

[References](#)

[Tables](#)

[Figures](#)

◀

▶

◀

▶

[Back](#)

[Close](#)

[Full Screen / Esc](#)

[Printer-friendly Version](#)

[Interactive Discussion](#)



Model simulated trend of surface carbon monoxide

J. Yoon and A. Pozzer

[Title Page](#)

[Abstract](#)

[Introduction](#)

[Conclusions](#)

[References](#)

[Tables](#)

[Figures](#)

◀

▶

[Back](#)

[Close](#)

[Full Screen / Esc](#)

[Printer-friendly Version](#)

[Interactive Discussion](#)



Crutzen, P. J. and Gidel, L. T.: A two-dimensional photochemical model of the atmosphere., 2: The tropospheric budgets of anthropogenic chlorocarbons CO, CH₄, CH₃Cl and the effect of various NO_x sources on tropospheric ozone, *J. Geophys. Res.*, 88, 6641–6661, 1983.

5 Davidson, E. A. and Artaxo, P.: Globally significant changes in biological processes of the Amazon Basin: results of the Large-scale Biosphere-Atmosphere Experiment, *Glob. Change Biol.*, 10, 1–11, doi:10.1111/j.1529-8817.2003.00779.x, 2004.

Deeter, M. N., Emmons, L. K., Francis, G. L., Edwards, D. P., Gille, J. C., Warner, J. X., Khattatov, B., Ziskin, D., Lamarque, J.-F., Ho, S.-P., Yudin, V., Attié, J.-L., Packman, D., Chen, J., Mao, D., and Drummond, J. R.: Operational carbon monoxide retrieval algorithm and selected results for the MOPITT instrument, *J. Geophys. Res.*, 108, D14, 4399, doi:10.1029/2002JD003186, 2003.

Deeter, M. N., Edwards, D. P., Gille, J. C., and Drummond, J. R.: Sensitivity of MOPITT observations to carbon monoxide in the lower troposphere. *J. Geophys. Res.*, 112, 24306, doi:10.1029/2007JD008929, 2007.

15 Deeter, M. N., Worden, H. M., Gille, J. C., Edwards, D. P., Mao, D., and Drummond, J. R.: MOPITT multispectral CO retrievals: origins and effects of geophysical radiance errors, *J. Geophys. Res.*, 116, D15303, doi:10.1029/2011JD015703, 2011.

Deeter, M. N., Worden, H. M., Edwards, D. P., Gille, J. C., and Andrews, A. E.: Evaluation of MOPITT retrievals of lower-tropospheric carbon monoxide over the United States, *J. Geophys. Res.*, 117, D13306, doi:10.1029/2012JD017553, 2012.

20 Deeter, M. N., Martínez-Alonso, S., Edwards, D. P., Emmons, L. K., Gille, J. C., Worden, H. M., Pittman, J. V., Daube, B. C., and Wofsy, S. C.: Validation of MOPITT Version 5 thermal-infrared, near-infrared, and multispectral carbon monoxide profile retrievals for 2000–2011, *J. Geophys. Res.*, 118, 1–16, doi:10.1002/jgrd.50272, 2013.

25 de Laat, A. T. J., Gloudemans, A. M. S., Aben, I., Krol, M., Meirink, J. F., van der Werf, G. R., and Schrijver, H.: Scanning Imaging Absorption Spectrometer for Atmospheric Chartography carbon monoxide total columns: statistical evaluation and comparison with chemistry transport model results, *J. Geophys. Res.*, 112, D12310, doi:10.1029/2006JD008256, 2007.

de Meij, A., Pozzer, A., and Lelieveld, J.: Trend analysis in aerosol optical depths and pollutant emission estimates between 2000 and 2009, *Atmos. Environ.*, 51, 75–85, doi:10.1016/j.atmosenv.2012.01.059, 2012.

30 Dlugokencky, E. J., Dutton, E. G., Novelli, P. C., Tans, P. P., Masarie, K. A., Lantz, K. O., and Madronich, S.: Changes in methane and CO growth rates after the eruption of Mt. Pinatubo

and their link with changes in tropical tropospheric UV flux, *Geophys. Res. Lett.*, 23, 2761–2764, doi:10.1029/96GL02638, 1996.

Drummond, J. R. and Mand, G. S.: The measurements of pollution in the troposphere (MOPITT) instrument: overall performance and calibration requirements, *J. Atmos. Ocean Tech.*, 13, 314–320, 1996.

Duncan, B. N. and Logan, J. A.: Model analysis of the factors regulating the trends and variability of carbon monoxide between 1988 and 1997, *Atmos. Chem. Phys.*, 8, 7389–7403, doi:10.5194/acp-8-7389-2008, 2008.

Duncan, B. N., Logan, J. A., Megretskaya, I. A., Yantosca, R. M., Novelli, P. C., Jones, N. B., and Rinsland, C. P.: The global budget of CO, 1988–1997: source estimates and validation with a global model, *J. Geophys. Res.-Atmos.*, 112, D22301, doi:10.1029/2007JD008459, 2007.

Eltahir, E. A. B. and Bras, R. L.: Precipitation recycling, *Rev. Geophys.*, 34, 367–378, doi:10.1029/96RG01927, 1996.

Emmons, L. K., Deeter, M. N., Gille, J. C., Edwards, D. P., Attié, J.-L., Warner, J., Ziskin, D., Francis, G., Khattatov, B., Yudin, V., Lamarque, J.-F., Ho, S.-P., Mao, D., Chen, J. S., Drummond, J., Novelli, P., Sachse, G., Coffey, M. T., Hannigan, J. W., Gerbig, C., Kawakami, S., Kondo, Y., Takegawa, N., Schlager, H., Baehr, J., and Ziereis, H.: Validation of Measurements of Pollution in the Troposphere (MOPITT) CO retrievals with aircraft in situ profiles, *J. Geophys. Res.*, 109, D03309, doi:10.1029/2003JD004101, 2004.

Eskes, H. J. and Boersma, K. F.: Averaging kernels for DOAS total-column satellite retrievals, *Atmos. Chem. Phys.*, 3, 1285–1291, doi:10.5194/acp-3-1285-2003, 2003.

Facchini, M. C., Decesari, S., Mircea, M., Fuzzi, S., and Loglio, G.: Surface tension of atmospheric wet aerosol and cloud/fog droplets in relation to their organic carbon content and chemical composition, *Atmos. Environ.*, 33, 4853–4857, 2000.

Fishman, J. and Crutzen, P. J.: the origin of ozone in the troposphere, *Nature*, 274, 855–858, 1978.

Forster, P., Ramaswamy, V., Artaxo, P., Berntsen, T., Betts, R., Fahey, D. W., Haywood, J., Lean, J., Lowe, D. C., Myhre, G., Nganga, J., Prinn, R., Raga, G., Schulz, M., and Van Dorland, R.: Changes in Atmospheric Constituents and in Radiative Forcing. in: *Climate Change 2007: The Physical Science Basis. Contribution of Working Group I to the Fourth Assessment Report of the Intergovernmental Panel on Climate Change*, edited by: Solomon, S., Qin, D., Manning, M., Chen, Z., Marquis, M., Averyt, K. B., Tignor, M., and Miller, H. L., Cambridge University Press, Cambridge, UK and New York, NY, USA, 129–234, 2007.

Model simulated trend of surface carbon monoxide

J. Yoon and A. Pozzer

[Title Page](#)[Abstract](#)[Introduction](#)[Conclusions](#)[References](#)[Tables](#)[Figures](#)[◀](#)[▶](#)[◀](#)[▶](#)[Back](#)[Close](#)[Full Screen / Esc](#)[Printer-friendly Version](#)[Interactive Discussion](#)

Model simulated
trend of surface
carbon monoxide

J. Yoon and A. Pozzer

Title Page

Abstract

Introduction

Conclusions

References

Tables

Figures

◀

▶

Back

Close

Full Screen / Esc

Printer-friendly Version

Interactive Discussion



Fujino, J., Nair, R., Kainuma, M., Masui, T., and Matsuoka, Y.: Multi-gas mitigation analysis on stabilization scenarios using aim global model, *Energ. J.*, Special issue #3, 343–354, doi:10.5547/ISSN0195-6574-EJ-VolSI2006-NoSI3-17, 2006.

George, M., Clerbaux, C., Hurtmans, D., Turquety, S., Coheur, P.-F., Pommier, M., Hadji-Lazaro, J., Edwards, D. P., Worden, H., Luo, M., Rinsland, C., and McMillan, W.: Carbon monoxide distributions from the IASI/METOP mission: evaluation with other space-borne remote sensors, *Atmos. Chem. Phys.*, 9, 8317–8330, doi:10.5194/acp-9-8317-2009, 2009.

Giglio, L., Randerson, J. T., van der Werf, G. R., Kasibhatla, P. S., Collatz, G. J., Morton, D. C., and DeFries, R. S.: Assessing variability and long-term trends in burned area by merging multiple satellite fire products, *Biogeosciences*, 7, 1171–1186, doi:10.5194/bg-7-1171-2010, 2010.

Gomez-Pelaez, A. J., Ramos, R., Gomez-Trueba, V., Novelli, P. C., and Campo-Hernandez, R.: A statistical approach to quantify uncertainty in carbon monoxide measurements at the Izaña global GAW station: 2008–2011, *Atmos. Meas. Tech.*, 6, 787–799, doi:10.5194/amt-6-787-2013, 2013.

Granier, C., Bessagnet, B., Bond, T., D'Angiola, A., van der Gon, H. D., Frost, G. J., Heil, A., Kaiser, J. W., Kinne, S., Klimont, Z., Kloster, S., Lamarque, J.-F., Liousse, C., Masui, T., Meleux, F., Mieville, A., Ohara, T., Raut, J.-C., Riahi, K., Schultz, M. G., Smith, S. J., Thompson, A., van Aardenne, J., van der Werf, G. R., and van Vuuren, D. P.: Evolution of anthropogenic and biomass burning emissions of air pollutants at global and regional scales during the 1980–2010 period, *Climatic Change*, 109, 163–190, doi:10.1007/s10584-011-0154-1, 2011.

Graniera, C., Müller, J. F., Pétron, G., and Brasseur, G.: A three-dimensional study of the global CO budget, *Chemosphere*, 1, 255–261, doi:10.1016/S1465-9972(99)00007-0, 1999.

Haas-Laursea, D. and Hartley, D.: Consistent sampling methods for comparing models to CO₂ flask data, *J. Geophys. Res.*, 102, 19059–19071, doi:10.1029/97JD00795, 1997.

Hauglustaine, D. A., Brasseur, G. P., Walters, S., Rasch, P. J., Müller, J.-F., Emmons, L. K., and Carroll, M. A.: MOZART, a global chemical transport model for ozone and related chemical tracers: 2. Model results and evaluation, *J. Geophys. Res.*, 103, D21, 28291–28335, doi:10.1029/98JD02398, 1998.

Held, I. M., Delworth, T. L., Lu, J., Findell, K. L., and Knutson, T. R.: Simulation of Sahel drought in the 20th and 21st centuries, *P. Natl. Acad. Sci. USA*, 102, 17891–17896, doi:10.1073/pnas.0509057102, 2005.

- Hijjoka, Y., Matsuoka, Y., Nishimoto, H., Masui, M., and Kainuma, M.: Global GHG emissions scenarios under GHG concentration stabilization targets, *J. Global Environ. Eng.*, 13, 97–108, 2008.
- Hilboll, A., Richter, A., and Burrows, J. P.: Long-term changes of tropospheric NO₂ over megacities derived from multiple satellite instruments, *Atmos. Chem. Phys.*, 13, 4145–4169, doi:10.5194/acp-13-4145-2013, 2013.
- Ho, S.-P., Edwards, D. P., Gille, J. C., Luo, M., Osterman, G. B., Kulawik, S. S., and Worden, H.: A global comparison of carbon monoxide profiles and column amounts from Tropospheric Emission Spectrometer (TES) and Measurements of Pollution in the Troposphere (MOPITT), *J. Geophys. Res.*, 114, D21307, doi:10.1029/2009JD012242, 2009.
- Hogrefe, C., Lynn, B., Civerolo, K., Ku, J., Rosenthal, J., Rosenzweig, C., Goldberg, R., Gaffin, S., Knowlton, K., and Kinney, P.: Simulating changes in regional air pollution over the eastern United States due to changes in global and regional climate and emissions, *J. Geophys. Res.*, 109, D22301, doi:10.1029/2004JD004690, 2004.
- Intergovernmental Panel on Climate Change (IPCC): *Climate Change 1995*, University Press, Cambridge, UK, 1996.
- Hsu, N. C., Gautam, R., Sayer, A. M., Bettenhausen, C., Li, C., Jeong, M. J., Tsay, S.-C., and Holben, B. N.: Global and regional trends of aerosol optical depth over land and ocean using SeaWiFS measurements from 1997 to 2010, *Atmos. Chem. Phys.*, 12, 8037–8053, doi:10.5194/acp-12-8037-2012, 2012.
- Ehhalt, D., Prather, M., Dentener, F., Derwent, R., Dlugokencky, E., Holland, E., Isaksen, I., Katima, J., Kirchhoff, V., Matson, P., Midgley, P., and Wang, M.: Atmospheric chemistry and greenhouse gases, in: *Climate Change 2001: The Scientific Basis, Contribution of Working Group I to the Third Assessment Report of the Intergovernmental Panel on Climate Change*, edited by: Houghton, J. T., Ding, Y., Griggs, D. J., Noguer, M., van der Linden, P. J., Dai, X., Maskell, K., and Johnson, C. A., Cambridge University Press, Cambridge, UK, 257–259, 2001.
- Jacobson, M. and Streets, D.: Influence of future anthropogenic emissions on climate, natural emissions, and air quality, *J. Geophys. Res.*, 114, D08118, doi:10.1029/2008JD011476, 2009.
- Jeuken, A. B. M., Siegmund, P. C., Heijboer, L. C., Feichter, J., and Bengtsson, L.: On the potential of assimilating meteorological analyses in a global climate model for the purpose of model validation, *J. Geophys. Res.*, 101, 16939–16950, doi:10.1029/96JD01218, 1996.

Model simulated trend of surface carbon monoxide

J. Yoon and A. Pozzer

[Title Page](#)[Abstract](#)[Introduction](#)[Conclusions](#)[References](#)[Tables](#)[Figures](#)[◀](#)[▶](#)[◀](#)[▶](#)[Back](#)[Close](#)[Full Screen / Esc](#)[Printer-friendly Version](#)[Interactive Discussion](#)

Model simulated trend of surface carbon monoxide

J. Yoon and A. Pozzer

- Jöckel, P., Tost, H., Pozzer, A., Brühl, C., Buchholz, J., Ganzeveld, L., Hoor, P., Kerkweg, A., Lawrence, M. G., Sander, R., Steil, B., Stiller, G., Tanarhte, M., Taraborrelli, D., van Aardenne, J., and Lelieveld, J.: The atmospheric chemistry general circulation model ECHAM5/MESSy1: consistent simulation of ozone from the surface to the mesosphere, *Atmos. Chem. Phys.*, 6, 5067–5104, doi:10.5194/acp-6-5067-2006, 2006.
- Jöckel, P., Kerkweg, A., Pozzer, A., Sander, R., Tost, H., Riede, H., Baumgaertner, A., Gromov, S., and Kern, B.: Development cycle 2 of the Modular Earth Submodel System (MESSy2), *Geosci. Model Dev.*, 3, 717–752, doi:10.5194/gmd-3-717-2010, 2010.
- Johnson, B. T., Osborne, S. R., Haywood, J. M., and Harrison, M. A. J.: Aircraft measurements of biomass burning aerosol over West Africa during DABEX, *J. Geophys. Res.*, 113, D00C06, doi:10.1029/2007JD009451, 2008.
- Khalil, M. A. K. and Rasmussen, R. A.: Carbon monoxide in the Earth's atmosphere: indications of a global increase, *Nature*, 332, 242–245, doi:10.1038/332242a0, 1988.
- Khalil, M. A. K. and Rasmussen, R. A.: The global cycle of carbon monoxide: trends and mass balance, *Chemosphere*, 20, 227–242, 1990.
- Kirby, K. R., Laurance, W. F., Albernaz, A. K., Schroth, G., Fearnside, P. M., Bergen, S., Venticinque, E. M., and da Costa, C.: The future of deforestation in the Brazilian Amazon, *Futures*, 38, 432–453, doi:10.1016/j.futures.2005.07.011, 2006.
- Klonecki, A., Pommier, M., Clerbaux, C., Ancellet, G., Cammas, J.-P., Coheur, P.-F., Cozic, A., Diskin, G. S., Hadji-Lazaro, J., Hauglustaine, D. A., Hurtmans, D., Khattatov, B., Lamarque, J.-F., Law, K. S., Nedelec, P., Paris, J.-D., Podolske, J. R., Prunet, P., Schlager, H., Szopa, S., and Turquety, S.: Assimilation of IASI satellite CO fields into a global chemistry transport model for validation against aircraft measurements, *Atmos. Chem. Phys.*, 12, 4493–4512, doi:10.5194/acp-12-4493-2012, 2012.
- Kopacz, M., Jacob, D. J., Fisher, J. A., Logan, J. A., Zhang, L., Megretskaya, I. A., Yantosca, R. M., Singh, K., Henze, D. K., Burrows, J. P., Buchwitz, M., Khlystova, I., McMillan, W. W., Gille, J. C., Edwards, D. P., Eldering, A., Thouret, V., and Nedelec, P.: Global estimates of CO sources with high resolution by adjoint inversion of multiple satellite datasets (MOPITT, AIRS, SCIAMACHY, TES), *Atmos. Chem. Phys.*, 10, 855–876, doi:10.5194/acp-10-855-2010, 2010.
- Latif, M. and Keenlyside, N. S.: El Niño/Southern Oscillation response to global warming, *P. Natl. Acad. Sci. USA*, 106, 49, 20578–20583, doi:10.1073/pnas.0710860105, 2009.

[Title Page](#)

[Abstract](#)

[Introduction](#)

[Conclusions](#)

[References](#)

[Tables](#)

[Figures](#)

◀

▶

◀

▶

[Back](#)

[Close](#)

[Full Screen / Esc](#)

[Printer-friendly Version](#)

[Interactive Discussion](#)



Model simulated
trend of surface
carbon monoxide

J. Yoon and A. Pozzer

Title Page

Abstract

Introduction

Conclusions

References

Tables

Figures

◀

▶

Back

Close

Full Screen / Esc

Printer-friendly Version

Interactive Discussion



- Law, K. S.: Theoretical studies of carbon monoxide distributions, budgets and trends, *Chemosphere*, 1, 19–31, doi:10.1016/S1465-9972(99)00020-3, 1999.
- Lawrence, M. G., Jöckel, P., and von Kuhlmann, R.: What does the global mean OH concentration tell us?, *Atmos. Chem. Phys.*, 1, 37–49, doi:10.5194/acp-1-37-2001, 2001.
- 5 Leggett, J., Pepper, W. J., and Swart, R. J.: Emissions scenarios for the IPCC: an update, in: *Climate Change 1992: The Supplementary Report to the IPCC Scientific Assessment*, prepared by: IPCC Working Group I, edited by: Houghton, J. T., Callander, B. A., and Varney, S. K. and WMO/UNEP, Cambridge University Press, Cambridge, UK, and New York, NY, USA, 1992.
- 10 Lelieveld, J., Peters, W., Dentener, F. J., and Krol, M. C.: Stability of tropospheric hydroxyl chemistry, *J. Geophys. Res.*, 107, ACH 17-1–ACH 17-11, doi:10.1029/2002JD002272, 2002.
- Lelieveld, J., Dentener, F. J., Peters, W., and Krol, M. C.: On the role of hydroxyl radicals in the self-cleansing capacity of the troposphere, *Atmos. Chem. Phys.*, 4, 2337–2344, doi:10.5194/acp-4-2337-2004, 2004.
- 15 Lelieveld, J., Barlas, C., Giannadaki, D., and Pozzer, A.: Model calculated global, regional and megacity premature mortality due to air pollution, *Atmos. Chem. Phys.*, 13, 7023–7037, doi:10.5194/acp-13-7023-2013, 2013.
- Levy, H.: Normal atmosphere: large radical and formaldehyde concentrations predicted, *Science*, 173, 141–143, doi:10.1126/science.173.3992.141, 1971.
- 20 Li, W. and Fu, R.: Transition of the large-scale atmospheric and land surface conditions from dry to wet season over Amazonia as diagnosed by the ECMWF re-analysis, *J. Climate*, 17, 2637–2651, doi:10.1175/1520-0442(2004)017<2637:TOTLAA>2.0.CO;2, 2004.
- Logan, J. A., Prather, M. J., Wofsy, S. C., and McElroy, M. B.: Tropospheric chemistry: a global perspective, *J. Geophys. Res.*, 86, C8, 7210–7254, doi:10.1029/JC086iC08p07210, 1981.
- 25 Lu, Z., Streets, D. G., Zhang, Q., Wang, S., Carmichael, G. R., Cheng, Y. F., Wei, C., Chin, M., Diehl, T., and Tan, Q.: Sulfur dioxide emissions in China and sulfur trends in East Asia since 2000, *Atmos. Chem. Phys.*, 10, 6311–6331, doi:10.5194/acp-10-6311-2010, 2010.
- Luo, M., Rinsland, C. P., Rodgers, C. D., Logan, J. A., Worden, H., Kulawik, S., Eldering, A., Goldman, A., Shephard, M. W., Gunson, M., and Lampel, M.: TES carbon monoxide validation with DACOM aircraft measurements during INTEX-B 2006, *J. Geophys. Res.*, 112, D24S48, doi:10.1029/2007JD008803, 2007a.
- 30 Luo, M., Rinsland, C. P., Rodgers, C. D., Logan, J. A., Worden, H., Kulawik, S., Eldering, A., Goldman, A., Shephard, M. W., Gunson, M., and Lampel, M.: Comparison of carbon

Model simulated trend of surface carbon monoxide

J. Yoon and A. Pozzer

[Title Page](#)

[Abstract](#)

[Introduction](#)

[Conclusions](#)

[References](#)

[Tables](#)

[Figures](#)

[◀](#)

[▶](#)

[◀](#)

[▶](#)

[Back](#)

[Close](#)

[Full Screen / Esc](#)

[Printer-friendly Version](#)

[Interactive Discussion](#)



monoxide measurements by TES and MOPITT: influence of a priori data and instrument characteristics on nadir atmospheric species retrievals, *J. Geophys. Res.*, 112, D09303, doi:10.1029/2006JD007663, 2007b.

McFiggans, G., Alfarra, M., Allan, J., Bower, K., and Coe, H.: Simplification of the representation of the organic component of atmospheric particulates, *Faraday Discuss.*, 130, 341–362, doi:10.1039/b419435g, 2005.

McFiggans, G., Artaxo, P., Baltensperger, U., Coe, H., Facchini, M. C., Feingold, G., Fuzzi, S., Gysel, M., Laaksonen, A., Lohmann, U., Mentel, T. F., Murphy, D. M., O'Dowd, C. D., Snider, J. R., and Weingartner, E.: The effect of physical and chemical aerosol properties on warm cloud droplet activation, *Atmos. Chem. Phys.*, 6, 2593–2649, doi:10.5194/acp-6-2593-2006, 2006.

Meehl, G. A., Covey, C., Delworth, T., Latif, M., McAvaney, B., Mitchell, J. F. B., Stouffer, R. J., and Taylor, K. E.: The WCRP CMIP3 multimodel dataset: a new era in climate change research, *B. Am. Meteorol. Soc.*, 88, 1383–1394, doi:10.1175/BAMS-88-9-1383, 2007.

Meinshausen, M., Smith, S. J., Calvin, K., Daniel, J. S., Kainuma, M. L. T., Lamarque, J- F., Matsumoto, K., Montzka, S. A., Raper, S. C. B., Riahi, K., Thomson, A., Velders, G. J. M., and van Vuuren, D. P. P.: The RCP greenhouse gas concentrations and their extensions from 1765 to 2300, *Climatic Change*, 109, 1–2, 213–241, doi:10.1007/s10584-011-0156-z, 2011.

Nakicenovic, N., Alcamo, J., Davis, G., De Vries, B., Fenner, J., Gaffin, S., Gregory, K., Grübler, A., Jung, T. Y., Kram, T., Lebre La Rovere, E., Michaelis, L., Mori, S., Morita, T., Pepper, W., Pitcher, H., Price, L., Riahi, K., Roehrl, A., Rogner, H. H., Sankovski, A., Schlesinger, M., Priyadarshi Shukla, P., Smith, S., Swart, R., Van Rooijen, S., Victor, N., and Dadi, Z.: Special Report on Emissions Scenarios, Intergovernmental Panel on Climate Change, 599 pp., Cambridge University press, Cambridge, United Kingdom and New York, USA, 2000.

Nepstad, D., Veríssimo, A., Alencar, A., Nobres, C., Lima, E., Lefebvre, P., Schlesinger, P., Potter, C., Moutinho, P., Mendoza, E., Cochrane, M., and Brooks, V.: Large-scale impoverishment of Amazonian forests by logging and fire, *Nature*, 398, 505–508, 1999.

Novelli, P. C., Steele, L. P., and Tans, P. P.: Mixing ratios of carbon monoxide in the troposphere, *J. Geophys. Res.*, 97, 20731–20750, doi:10.1029/92JD02010, 1992.

Novelli, P. C., Masarie, K. A., Tans, P. P., and Lang, P. M.: Recent changes in atmospheric carbon monoxide, *Science*, 263, 1587–1590, doi:10.1126/science.263.5153.1587, 1994.

Model simulated
trend of surface
carbon monoxide

J. Yoon and A. Pozzer

Title Page

Abstract

Introduction

Conclusions

References

Tables

Figures

◀

▶

◀

▶

Back Close

Full Screen / Esc

Printer-friendly Version

Interactive Discussion



Novelli, P. C., Masarie, K. A., Lang, P. M., Hall, B. D., Myers, R. C., and Elkins, J. W.: Reanalysis of tropospheric CO trends: effects of the 1997–1998 wildfires, *J. Geophys. Res.*, 108, 4464, doi:10.1029/2002JD003031, 2003.

5 Ohara, T., Akimoto, H., Kurokawa, J., Horii, N., Yamaji, K., Yan, X., and Hayasaka, T.: An Asian emission inventory of anthropogenic emission sources for the period 1980–2020, *Atmos. Chem. Phys.*, 7, 4419–4444, doi:10.5194/acp-7-4419-2007, 2007.

Pan, L., Gille, J. C., Edwards, D. P., Bailey, P. L., and Rodgers, C. D.: Retrieval of tropospheric carbon monoxide for the MOPITT experiment, *J. Geophys. Res.*, 103, D24, 32277–32290, doi:10.1029/98JD01828, 1998.

10 Pozzer, A., Jöckel, P., Tost, H., Sander, R., Ganzeveld, L., Kerkweg, A., and Lelieveld, J.: Simulating organic species with the global atmospheric chemistry general circulation model ECHAM5/MESSy1: a comparison of model results with observations, *Atmos. Chem. Phys.*, 7, 2527–2550, doi:10.5194/acp-7-2527-2007, 2007.

15 Pozzer, A., Jöckel, P., and Van Aardenne, J.: The influence of the vertical distribution of emissions on tropospheric chemistry, *Atmos. Chem. Phys.*, 9, 9417–9432, doi:10.5194/acp-9-9417-2009, 2009.

20 Pozzer, A., de Meij, A., Pringle, K. J., Tost, H., Doering, U. M., van Aardenne, J., and Lelieveld, J.: Distributions and regional budgets of aerosols and their precursors simulated with the EMAC chemistry-climate model, *Atmos. Chem. Phys.*, 12, 961–987, doi:10.5194/acp-12-961-2012, 2012a.

Pozzer, A., Zimmermann, P., Doering, U.M., van Aardenne, J., Tost, H., Dentener, F., Janssens-Maenhout, G., and Lelieveld, J.: Effects of business-as-usual anthropogenic emissions on air quality, *Atmos. Chem. Phys.*, 12, 6915–6937, doi:10.5194/acp-12-6915-2012, 2012b.

25 Rasmusson, E. M. and Carpenter, T. H.: Variations in Tropical Sea Surface Temperature and Surface Wind Fields Associated with the Southern Oscillation/El Niño, *Mon. Weather Rev.*, 110, 354–384, doi:10.1175/1520-0493(1982)110<0354:VITSST>2.0.CO;2, 1982.

30 Reeves, C. E., Formenti, P., Afif, C., Ancellet, G., Attié, J.-L., Bechara, J., Borbon, A., Cairo, F., Coe, H., Crumeyrolle, S., Fierli, F., Flamant, C., Gomes, L., Hamburger, T., Jambert, C., Law, K. S., Mari, C., Jones, R. L., Matsuki, A., Mead, M. I., Methven, J., Mills, G. P., Minikin, A., Murphy, J. G., Nielsen, J. K., Oram, D. E., Parker, D. J., Richter, A., Schlager, H., Schwarzenboeck, A., and Thouret, V.: Chemical and aerosol characterisation of the troposphere over West Africa during the monsoon period as part of AMMA, *Atmos. Chem. Phys.*, 10, 7575–7601, doi:10.5194/acp-10-7575-2010, 2010.

Model simulated
trend of surface
carbon monoxide

J. Yoon and A. Pozzer

Title Page

Abstract

Introduction

Conclusions

References

Tables

Figures

◀

▶

◀

▶

Back Close

Full Screen / Esc

Printer-friendly Version

Interactive Discussion



- Riahi, K., Gruebler, A., and Nakicenovic, N.: Scenarios of long-term socio-economic and environmental development under climate stabilization, *Technol. Forecast. Soc. Change*, 74, 887–935, doi:10.1016/j.techfore.2006.05.026, 2007.
- Richter, A., Burrows, J. P., Nüß, H., Granier, C., and Niemeier, U.: Increase in tropospheric nitrogen dioxide over China observed from space, *Nature Lett.*, 437, 129–132, doi:10.1038/nature04092, 2005.
- Rieder, H. E., Frossard, L., Ribatet, M., Staehelin, J., Maeder, J. A., Di Rocco, S., Davison, A. C., Peter, T., Weihs, P., and Holawe, F.: On the relationship between total ozone and atmospheric dynamics and chemistry at mid-latitudes – Part 2: The effects of the El Niño/Southern Oscillation, volcanic eruptions and contributions of atmospheric dynamics and chemistry to long-term total ozone changes, *Atmos. Chem. Phys.*, 13, 165–179, doi:10.5194/acp-13-165-2013, 2013.
- Rodgers, C. D.: Inverse Methods for Atmospheric Sounding – Theory and Practice, Series on Atmospheric, Oceanic and Planetary Physics, World Scientific Publishing, Singapore, 2000.
- Rodgers, C. D. and Connor, B. J.: Intercomparison of remote sounding instruments, *J. Geophys. Res.*, D3, 4116, doi:10.1029/2002JD002299, 2003.
- Roeckner, E., Brokopf, R., Esch, M., Giorgetta, M., Hagemann, S., Kornblueh, L., Manzini, E., Schlese, U., and Schulzweida, U.: Sensitivity of simulated climate to horizontal and vertical resolution in the ECHAM5 atmosphere model, *J. Climate*, 19, 3771–3791, doi:10.1175/JCLI3824.1, 2006.
- Smith, S. J. and Wigley, T. M. L.: Multi-gas forcing stabilization with Minicam, *Energ. J.*, Special issue #3, 373–392, doi:10.5547/ISSN0195-6574-EJ-VolSI2006-NoSI3-19, 2006.
- Smith, S. J., Pitcher, H., and Wigley, T. M. L.: Global and regional anthropogenic sulfur dioxide emissions, *Glob. Planet. Change*, 29, 1–2, 99–119, doi:10.1016/S0921-8181(00)00057-6, 2001.
- Streets, D. G., Bond, T. C., Carmichael, G. R., Fernandes, S. D., Fu, Q., He, D., Klimont, Z., Nelson, S. M., Tsai, N. Y., Wang, M. Q., Woo, J.-H., and Yarber, K. F.: An inventory of gaseous and primary aerosol emissions in Asia in the year 2000, *J. Geophys. Res.*, 108, D21, 8809, doi:10.1029/2002JD003093, 2003.
- Streets, D. G., Wu, Y., and Chin, M.: Two-decadal aerosol trends as a likely explanation of the global dimming/brightening transition, *Geophys. Res. Lett.*, 33, L15806, doi:10.1029/2006GL026471, 2006.

Model simulated trend of surface carbon monoxide

J. Yoon and A. Pozzer

[Title Page](#)

[Abstract](#)

[Introduction](#)

[Conclusions](#)

[References](#)

[Tables](#)

[Figures](#)

◀

▶

[Back](#)

[Close](#)

[Full Screen / Esc](#)

[Printer-friendly Version](#)

[Interactive Discussion](#)



Susskind, J., Barnet, C. D., and Blaisdell, J. M.: Retrieval of atmospheric and surface parameters from AIRS/AMSU/HSB data in the presence of clouds, *IEEE T. Geosci. Remote*, 41, 390–409, 2003.

Taylor, K. E.: Summarizing multiple aspects of model performance in a single diagram, *J. Geophys. Res.*, 106, 7183–7192, doi:10.1029/2000JD900719, 2001.

Thompson, A. M.: The oxidizing capacity of the Earth's atmosphere – probable past and future changes, *Science*, 256, 1157–1165, doi:10.1126/science.256.5060.1157, 1992.

Thompson, A. M. and Cicerone, R. J.: Possible perturbations to atmospheric CO, CH₄, and OH, *J. Geophys. Res.*, 91, 10853–10864, doi:10.1029/JD091iD10p10853, 1986.

Tiao, G. C., Reinsel, G. C., Xu, D., Pedrick, J. H., Zhu, X., Miller, A. J., DeLuisi, J. J., Mateer, C. L., and Wuebbles, D. J.: Effects of autocorrelation and temporal sampling schemes on estimates of trend and spatial correlation, *J. Geophys. Res.*, 95, 20507–20517, doi:10.1029/JD095iD12p20507, 1990.

Tohjima, Y., Kubo, M., Minejima, C., Mukai, H., Tanimoto, H., Ganshin, A., Maksyutov, S., Katsumata, K., Machida, T., and Kita, K.: Temporal changes in the emissions of CH₄ and CO from China estimated from CH₄/CO₂ and CO/CO₂ correlations observed at Hateruma Island, *Atmos. Chem. Phys.*, 14, 1663–1677, doi:10.5194/acp-14-1663-2014, 2014.

Trenberth, K. E., Caron, J. M., Stepaniak, D. P., and Worley, S.: Evolution of El Niño-Southern Oscillation and global atmospheric surface temperatures, *J. Geophys. Res.*, 107, 4065, doi:10.1029/2000JD000298, 2002.

van der Werf, G. R., Randerson, J. T., Giglio, L., Collatz, G. J., Mu, M., Kasibhatla, P. S., Morton, D. C., DeFries, R. S., Jin, Y., and van Leeuwen, T. T.: Global fire emissions and the contribution of deforestation, savanna, forest, agricultural, and peat fires (1997–2009), *Atmos. Chem. Phys.*, 10, 11707–11735, doi:10.5194/acp-10-11707-2010, 2010.

van Vuuren, D. P., Eickhout, B., Lucas, P. L., and den Elzen, M. G. J.: Long-term multi-gas scenarios to stabilise radiative forcing – exploring costs and benefits within an integrated assessment framework, *Energ. J.*, Special issue #3, 201–234, doi:10.5547/ISSN0195-6574-EJ-VolSI2006-NoSI3-10, 2006.

van Vuuren, D. P., den Elzen, M. G. J., Lucas, P. L., Eickhout, B., Strengers, B. J., van Ruijven, B., Wonink, S., and van Houdt, R.: Stabilizing greenhouse gas concentrations at low levels: an assessment of reduction strategies and costs, *Climatic Change*, 81, 119–159, doi:10.1007/s10584-006-9172-9, 2007.

- van Vuuren, D. P., Edmonds, J. A., Kainuma, M., Riahi, K., Thomson, A. M., Hibbard, K., Hurtt, G. C., Kram, T., Krey, V., Lamarque, J.-F., Masui, T., Nakicenovic, M. M. N., Smith, S. J., and Rose, S.: The representative concentration pathways: an overview, *Climatic Change*, 109, 5–31, doi:10.1007/s10584-011-0148-z, 2011.
- 5 Wallace, J. M. and Hobbs, P. V.: *Atmospheric Chemistry*. in: *Atmospheric Science*, Second Edition: an Introductory Survey, edited by: Dmowska, R., Hartmann, D., and Rossby, H. T., Elsevier, MA, USA, California, USA, and London, UK, 153–207, 2006.
- 10 Warner, J. X., McCourt Comer, M., Barnet, C., McMillan, W. W., Wolf, W., Maddy, E., and Sachse, G.: A Comparison of Satellite Tropospheric Carbon Monoxide Measurements from AIRS and MOPITT During INTEX-NA, *J. Geophys. Res.*, 112, D12S1, doi:10.1029/2006JD007925, 2007.
- 15 Warner, J. X., Wei, Z., Strow, L. L., Barnet, C. D., Sparling, L. C., Diskin, G., and Sachse, G.: Improved agreement of AIRS tropospheric carbon monoxide products with other EOS sensors using optimal estimation retrievals, *Atmos. Chem. Phys.*, 10, 9521–9533, doi:10.5194/acp-10-9521-2010, 2010.
- 20 Weatherhead, E. C., Reinsel, G. C., Tiao, G. C., Meng, X.-L., Choi, D., Cheang, W.-K., Keller, T., DeLuisi, J., Wuebbles, D. J., Kerr, J. B., Miller, A. J., Oltmans, S. J., and Frederick, J. E.: Factors affecting the detection of trends: statistical considerations and applications to environmental data, *J. Geophys. Res.*, 103, 17149–17161, doi:10.1029/98JD00995, 1998.
- 25 Weatherhead, E. C., Stevermer, A. J., and Schwartz, B. E.: Detecting environmental changes and trends, *Phys. Chem. Earth*, 27, 399–403, doi:10.1016/S1474-7065(02)00019-0, 2002.
- Wise, M., Calvin, K., Thomson, A., Clarke, L., Bond-Lamberty, B., Sands, R., Smith, S. J., Janetos, A., and Edmonds, J.: Implications of limiting CO₂ concentrations for land use and energy, *Science*, 324, 5931, 1183–1186, doi:10.1126/science.1168475, 2009.
- 30 WMO: Scientific Assessment of Ozone Depletion: 1998, Global Ozone Research and Monitoring Project – Report No. 44, World Meteorological Organization, Geneva, Switzerland, 732 pp., 1999.
- WMO: Revision of the World Data Centre for Greenhouse Gases Data Submission and Dissemination Guide, GAW Report No. 188, WMO TD No.1507, World Meteorological Organization, Geneva, Switzerland, 49 pp., 2009.
- Worden, H. M., Deeter, M. N., Edwards, D. P., Gille, J. C., Drummond, J. R., and Nédélec, P. P.: Observations of near-surface carbon monoxide from space using MOPITT multispectral retrievals, *J. Geophys. Res.*, 115, D18314, doi:10.1029/2010JD014242, 2010.

[Title Page](#)[Abstract](#)[Introduction](#)[Conclusions](#)[References](#)[Tables](#)[Figures](#)[◀](#)[▶](#)[◀](#)[▶](#)[Back](#)[Close](#)[Full Screen / Esc](#)[Printer-friendly Version](#)[Interactive Discussion](#)

- Worden, H. M., Deeter, M. N., Frankenberg, C., George, M., Nichitiu, F., Worden, J., Aben, I., Bowman, K. W., Clerbaux, C., Coheur, P. F., de Laat, A. T. J., Detweiler, R., Drummond, J. R., Edwards, D. P., Gille, J. C., Hurtmans, D., Luo, M., Martínez-Alonso, S., Massie, S., Pfister, G., and Warner, J. X.: Decadal record of satellite carbon monoxide observations, *Atmos. Chem. Phys.*, 13, 837–850, doi:10.5194/acp-13-837-2013, 2013.
- Xu, X., Lin, W., Wang, T., Yan, P., Tang, J., Meng, Z., and Wang, Y.: Long-term trend of surface ozone at a regional background station in eastern China 1991–2006: enhanced variability, *Atmos. Chem. Phys.*, 8, 2595–2607, doi:10.5194/acp-8-2595-2008, 2008.
- Yoon, J., von Hoyningen-Huene, W., Vountas, M., and Burrows, J. P.: Analysis of linear long-term trend of aerosol optical thickness derived from SeaWiFS using BAER over Europe and South China, *Atmos. Chem. Phys.*, 11, 12149–12167, doi:10.5194/acp-11-12149-2011, 2011.
- Yoon, J., von Hoyningen-Huene, W., Kokhanovsky, A. A., Vountas, M., and Burrows, J. P.: Trend analysis of aerosol optical thickness and Ångström exponent derived from the global AERONET spectral observations, *Atmos. Meas. Tech.*, 5, 1271–1299, doi:10.5194/amt-5-1271-2012, 2012.
- Yoon, J., Pozzer, A., Hoor, P., Chang, D. Y., Beirle, S., Wagner, T., Schloegl, S., Lelieveld, J., and Worden, H. M.: Technical Note: Temporal change in averaging kernels as a source of uncertainty in trend estimates of carbon monoxide retrieved from MOPITT, *Atmos. Chem. Phys.*, 13, 11307–11316, doi:10.5194/acp-13-11307-2013, 2013a.
- Yoon, J., Burrows, J. P., Vountas, M., von Hoyningen-Huene, W., Chang, D. Y., Richter, A., and Hilboll, A.: Changes in atmospheric aerosol loading retrieved from space based measurements during the past decade, *Atmos. Chem. Phys. Discuss.*, 13, 26001–26041, doi:10.5194/acpd-13-26001-2013, 2013b.
- Zhao, T. X.-P., Laszlo, I., Guo, W., Heidinger, A., Cao, C., Jelenak, A., Tarpley, D., and Sullivan, J.: Study of long-term trend in aerosol optical thickness observed from operational AVHRR satellite instrument, *J. Geophys. Res.*, 113, D07201, doi:10.1029/2007JD009061, 2008.
- Zhang, Y., Yu, H., Eck, T. F., Smirnov, A., Chin, M., Remer, L. A., Bian, H., Tan, Q., Levy, R., Holben, B. N., and Piazzolla, S.: Aerosol daytime variations over North and South America derived from multiyear AERONET measurements, *J. Geophys. Res.*, 117, D05211, doi:10.1029/2011JD017242, 2012.

**Model simulated
trend of surface
carbon monoxide**

J. Yoon and A. Pozzer

[Title Page](#)[Abstract](#)[Introduction](#)[Conclusions](#)[References](#)[Tables](#)[Figures](#)[◀](#)[▶](#)[◀](#)[▶](#)[Back](#)[Close](#)[Full Screen / Esc](#)[Printer-friendly Version](#)[Interactive Discussion](#)

Model simulated trend of surface carbon monoxide

J. Yoon and A. Pozzer

Table 1. Geolocation and abbreviation of the regions for evaluating the spatial distribution and estimating the regional/global trend of EMAC-simulated surface CO.

Region	Abbreviation	Latitude range	Longitude range
a. Pacific Region	PAR	10–30° N	165–145° W
b. Eastern USA	EUSA	25–45° N	90–70° W
c. Central South America	CSA	18–5° S	80–35° W
d. Western Europe	WE	35–60° N	10–15° E
e. Central AFrica	CAF	3–15° N	18–53° E
f. Southern AFrica	SAF	20–3° S	8–42° E
g. South Asia	SA	5–33° N	65–92° E
h. East China	EC	22–43° N	95–124° E
i. SouthEast Asia	SEA	10° S–20° N	95–120° E
j. Northern Australia	NA	20–11° S	120–150° E
k. Northern Hemisphere	NH	0–90° N	180° W–180° E
l. Sothern Hemisphere	SH	90° S–0° N	180° W–180° E
m. GLobe	GL	90° S–90° N	180° W–180° E

**Model simulated
trend of surface
carbon monoxide**

J. Yoon and A. Pozzer

Title Page

Abstract

Introduction

Conclusions

References

Tables

Figures

|◀

▶|

Back

Close

Full Screen / Esc

Printer-friendly Version

Interactive Discussion

Table 2. WDCGG stations providing full 10 year monthly records of surface CO from 2001 to 2010. The WDCGG-archived data are used for the evaluation of trend estimates in this study.

Station name	Latitude	Longitude	Country/Territory	Contributor ^a	Measurement Method ^b
Alert	82.5° N	62.5° W	Canada	CSIRO	RGD
Ascension Island	7.9° S	14.4° W	UK	NOAA/ESRL	GC-HgO
Assekrem	23.3° N	5.6° E	Algeria	NOAA/ESRL	GC-HgO
Barrow	71.3° N	156.6° W	USA	NOAA/ESRL	GC-HgO
Cape Ferguson	19.3° S	147.1° E	Australia	CSIRO	RGD
Cape Grim	40.7° S	144.7° E	Australia	CSIRO	RGD
Cape Grim	40.7° S	144.7° E	Australia	NOAA/ESRL	GC-HgO
Cape Point	34.4° S	18.5° E	South Africa	SAWS	GC-other
Casey Station	66.3° S	110.5° E	Australia	CSIRO	RGD
Halley Bay	75.6° S	26.5° W	UK	NOAA/ESRL	GC-HgO
Hegyhatsal	47.0° N	16.7° E	Hungary	NOAA/ESRL	GC-HgO
Heimaey	63.4° N	20.3° W	Iceland	NOAA/ESRL	GC-HgO
Izaña (Tenerife)	28.3° N	16.5° W	Spain	NOAA/ESRL	GC-HgO
Key Biscayne	25.7° N	80.2° W	USA	NOAA/ESRL	GC-HgO
Mace Head	53.3° N	9.9° W	Ireland	AGAGE	GC-MD
Mace Head	53.3° N	9.9° W	Ireland	NOAA/ESRL	GC-HgO
Macquarie Island	54.5° S	159.0° E	Australia	CSIRO	RGD
Mahe Island	4.7° S	55.2° E	Seychelles	NOAA/ESRL	GC-HgO
Mauna Loa	19.5° N	155.6° W	USA	NOAA/ESRL	GC-HgO
Mt. Waliguan	36.23° N	100.9° E	China	NOAA/ESRL, CMA	GC-HgO

^a CSIRO: Commonwealth Scientific and Industrial Research Organisation (<http://www.csiro.au/>), NOAA/ESRL: National Oceanic and Atmospheric Administration/Earth System Research Laboratory (<http://www.esrl.noaa.gov/>), SAWS: South African Weather Service (<http://www.weathersa.co.za/web/index.php>), AGAGE: Advanced Global Atmospheric Gases Experiment (<http://agage.eas.gatech.edu/>), CMA: China Meteorological Administration (<http://www.cma.gov.cn/en/>), JMA: Japan Meteorological Agency (<http://www.jma.go.jp/jma/indexe.html>), Empa: Swiss Federal Laboratories for Materials Science and Technology (German acronym for Eidgenössische Materialprüfungs- und Forschungsanstalt) (<http://www.empa.ch>)

^b RGD: Reduction Gas Detector, GC-HgO: Gas Chromatography – Mercuric Oxide Reduction Detection, GC-MD: Gas Chromatography – MultiDetector, GC-other: Gas Chromatography (other), NDIR: Non-Dispersive InfraRed gas analyzer



Table 2. Continued.

Station name	Latitude	Longitude	Country/Territory	Contributor ^a	Measurement Method ^b
Niwot Ridge (T-van)	40.1° N	105.6° W	USA	NOAA/ESRL	GC-HgO
Park Falls	45.9° N	90.3° W	USA	NOAA/ESRL	GC-HgO
Palmer Station	64.9° S	64.0° W	USA	NOAA/ESRL	GC-HgO
Payerne	46.8° N	7.0° E	Switzerland	Empa	NDIR
Point Arena	39.0° N	123.7° W	USA	NOAA/ESRL	GC-HgO
Ragged Point	13.2° N	59.4° W	Barbados	NOAA/ESRL	GC-HgO
Rigi	46.1° N	8.5° E	Switzerland	Empa	NDIR
Ryori	39.0° N	141.8° E	Japan	JMA	RGD
Sand Island	28.2° N	177.4° W	USA	NOAA/ESRL	GC-HgO
Sede Boker	31.1° N	34.9° E	Israel	NOAA/ESRL	GC-HgO
South Pole	90.0° S	24.8° W	USA	CSIRO	RGD
South Pole	90.0° S	24.8° W	USA	NOAA/ESRL	GC-HgO
Syowa Station	69.0° S	39.6° E	Japan	NOAA/ESRL	GC-HgO
Tae-ahn Peninsula	36.7° N	126.1° E	Republic of Korea	NOAA/ESRL	GC-HgO
Tudor Hill	32.3° N	64.9° W	UK	NOAA/ESRL	GC-HgO
Tutuila (Cape Matatula)	14.2° S	170.6° W	USA	NOAA/ESRL	GC-HgO
Ulaan Uul	44.5° N	111.1° E	Mongolia	NOAA/ESRL	GC-HgO
Wendover	39.9° N	-113.7° W	USA	NOAA/ESRL	GC-HgO
Yonagunijima	24.5° N	123.0° E	Japan	JMA	RGD
Zeppelinfjellet (Ny-Alesund)	79.0° N	11.9° E	Norway	NOAA/ESRL	GC-HgO

^a CSIRO: Commonwealth Scientific and Industrial Research Organisation (<http://www.csiro.au/>), NOAA/ESRL: National Oceanic and Atmospheric Administration/Earth System Research Laboratory (<http://www.esrl.noaa.gov/>), SAWS: South African Weather Service (<http://www.weathersa.co.za/web/index.php>), AGAGE: Advanced Global Atmospheric Gases Experiment (<http://agage.eas.gatech.edu/>), CMA: China Meteorological Administration (<http://www.cma.gov.cn/en/>), JMA: Japan Meteorological Agency (<http://www.jma.go.jp/jma/indexe.html>), Empa: Swiss Federal Laboratories for Materials Science and Technology (German acronym for Eidgenössische Materialprüfungs- und Forschungsanstalt) (<http://www.empa.ch/>)

^b RGD: Reduction Gas Detector, GC-HgO: Gas Chromatography – Mercuric Oxide Reduction Detection, GC-MD: Gas Chromatography – MultiDetector, GC-other: Gas Chromatography (other), NDIR: Non-Dispersive InfraRed gas analyzer

Model simulated trend of surface carbon monoxide

J. Yoon and A. Pozzer

[Title Page](#)

[Abstract](#)

[Introduction](#)

[Conclusions](#)

[References](#)

[Tables](#)

[Figures](#)

◀

▶

◀

▶

[Back](#)

[Close](#)

[Full Screen / Esc](#)

[Printer-friendly Version](#)

[Interactive Discussion](#)



Table 3. Means (CO) and corresponding statistic quantities* used in the comparison of spatial patterns (i.e. Taylor diagram in Figure 6.) between MOPITT-retrieved surface CO and pseudo-retrievals of EMAC-simulated surface CO.

Region	MOPITT-retrieved surface CO		Pseudo-retrieval of EMAC-simulated surface CO based on CE scenario				
	CO [ppbv]	σ [ppbv]	CO [ppbv]	σ [ppbv]	R [unitless]	RMS [ppbv]	B [%]
PAR	91.78 ± 33.49	7.32 ± 5.28	78.05 ± 15.88	3.28 ± 2.82	0.45 ± 0.63	6.53 ± 5.86	-14.97 ± 15.72
EUSA	212.59 ± 83.20	68.62 ± 20.38	156.62 ± 24.81	56.16 ± 23.11	0.83 ± 0.23	37.81 ± 30.95	-26.33 ± 23.90
CSA	113.29 ± 78.23	38.85 ± 66.01	111.38 ± 56.94	35.71 ± 50.32	0.92 ± 0.12	15.59 ± 23.14	-1.68 ± 16.39
WE	159.28 ± 47.53	30.35 ± 18.35	127.78 ± 25.46	27.74 ± 22.21	0.67 ± 0.42	23.56 ± 16.71	-19.78 ± 12.39
CAF	144.80 ± 89.62	48.61 ± 66.40	145.30 ± 88.66	63.57 ± 102.14	0.89 ± 0.15	30.55 ± 41.63	+0.35 ± 18.07
SAF	131.09 ± 83.03	45.83 ± 49.46	129.09 ± 61.08	44.95 ± 46.05	0.77 ± 0.36	30.86 ± 34.40	-1.53 ± 23.09
SA	148.30 ± 97.91	47.01 ± 30.33	125.09 ± 63.00	37.44 ± 25.01	0.87 ± 0.12	23.52 ± 20.34	-15.65 ± 19.05
EC	251.16 ± 97.49	105.37 ± 51.19	176.03 ± 49.78	77.18 ± 39.77	0.74 ± 0.14	70.42 ± 39.08	-29.91 ± 14.74
SEA	132.01 ± 52.60	61.51 ± 50.05	133.78 ± 33.34	57.43 ± 44.83	0.89 ± 0.12	27.85 ± 29.05	+1.34 ± 19.27
NA	90.60 ± 38.02	17.15 ± 14.18	89.12 ± 15.11	13.32 ± 7.23	0.82 ± 0.19	9.84 ± 11.35	-1.64 ± 26.81
NH	131.86 ± 40.93	48.95 ± 22.27	111.97 ± 24.17	39.46 ± 23.05	0.81 ± 0.13	28.90 ± 16.72	-15.08 ± 10.53
SH	67.89 ± 21.01	22.62 ± 19.06	73.08 ± 13.31	23.83 ± 13.33	0.86 ± 0.10	12.45 ± 6.67	+7.64 ± 13.67
GL	99.80 ± 13.54	50.98 ± 22.70	92.30 ± 6.52	38.52 ± 16.30	0.87 ± 0.06	25.99 ± 13.24	-7.51 ± 7.05
Region	Pseudo-retrieval of EMAC-simulated surface CO based on RG scenario						
	CO [ppbv]	σ [ppbv]	R [unitless]	RMS [ppbv]	B [%]		
PAR	86.66 ± 25.64	4.68 ± 4.47	0.69 ± 0.56	5.28 ± 3.23	-5.58 ± 10.06		
EUSA	197.96 ± 48.06	66.63 ± 16.25	0.96 ± 0.04	19.97 ± 12.95	-6.88 ± 17.85		
CSA	121.76 ± 82.84	45.99 ± 74.00	0.91 ± 0.13	19.14 ± 25.80	+7.48 ± 12.93		
WE	146.77 ± 36.01	28.22 ± 17.63	0.90 ± 0.12	13.15 ± 6.85	-7.85 ± 7.67		
CAF	154.74 ± 89.55	63.99 ± 96.87	0.93 ± 0.09	26.33 ± 32.73	+6.86 ± 18.10		
SAF	127.93 ± 67.17	47.06 ± 53.73	0.89 ± 0.12	21.34 ± 24.41	-2.41 ± 17.74		
SA	164.62 ± 107.02	64.56 ± 46.64	0.94 ± 0.05	25.36 ± 21.47	+11.00 ± 16.06		
EC	244.31 ± 83.70	107.22 ± 57.33	0.91 ± 0.06	45.32 ± 21.73	-2.73 ± 14.23		
SEA	144.45 ± 47.70	72.66 ± 76.01	0.94 ± 0.06	25.68 ± 46.89	+9.42 ± 15.39		
NA	91.07 ± 31.94	16.06 ± 13.43	0.84 ± 0.22	9.43 ± 6.72	+0.51 ± 17.14		
NH	125.14 ± 33.00	48.63 ± 27.50	0.93 ± 0.03	18.43 ± 8.82	-5.10 ± 7.94		
SH	66.16 ± 19.04	25.44 ± 21.77	0.94 ± 0.06	9.03 ± 9.26	-2.54 ± 5.23		
GL	95.52 ± 8.53	49.72 ± 20.84	0.95 ± 0.03	15.49 ± 5.17	-4.29 ± 5.58		

* The statistic quantities are the mean standard deviation (σ), spatial correlation coefficient (R), centred root-mean-square (RMS) difference, and relative bias (B) with a 95 % confidence interval.

Model simulated trend of surface carbon monoxide

J. Yoon and A. Pozzer

[Title Page](#)

[Abstract](#)

[Introduction](#)

[Conclusions](#)

[References](#)

[Tables](#)

[Figures](#)



[Full Screen / Esc](#)

[Printer-friendly Version](#)

[Interactive Discussion](#)



Model simulated trend of surface carbon monoxide

J. Yoon and A. Pozzer

Table 4. Trend estimate ($\hat{\omega}$) and corresponding significance value ($|\hat{\omega}/\sigma_{\hat{\omega}}|$) of the WDCGG-archived and EMAC-simulated surface CO at a 95 % confidence level.

Station	Contributor	WDCGG-archived surface CO		EMAC-simulated surface CO on CE scenario		EMAC-simulated surface CO on RG scenario	
		$\hat{\omega} \pm 2\sigma_{\hat{\omega}}$ [ppbvdecade $^{-1}$]	$ \hat{\omega}/\sigma_{\hat{\omega}} $ [unitless]	$\hat{\omega} \pm 2\sigma_{\hat{\omega}}$ [ppbvdecade $^{-1}$]	$ \hat{\omega}/\sigma_{\hat{\omega}} $ [unitless]	$\hat{\omega} \pm 2\sigma_{\hat{\omega}}$ [ppbvdecade $^{-1}$]	$ \hat{\omega}/\sigma_{\hat{\omega}} $ [unitless]
Alert	CSIRO	-26.29 ± 19.85	2.65	-1.40 ± 2.01	1.40	-15.75 ± 12.37	2.55
Ascension Island	NOAA/ESRL	+7.68 ± 5.99	2.56	-0.74 ± 2.19	0.68	+1.03 ± 4.29	0.48
Assekrem	NOAA/ESRL	-6.79 ± 6.89	1.97	-1.23 ± 3.30	0.75	-7.39 ± 4.64	3.19
Barrow	NOAA/ESRL	-15.01 ± 21.03	1.43	-1.32 ± 2.65	1.00	-14.22 ± 12.18	2.34
Cape Ferguson	CSIRO	-12.64 ± 10.26	2.47	-3.61 ± 3.58	2.01	-7.32 ± 5.71	2.56
Cape Grim	CSIRO	-6.02 ± 4.04	2.98	-1.40 ± 2.2	1.27	-2.79 ± 8.23	0.68
Cape Grim	NOAA/ESRL	+1.52 ± 5.06	0.60	-1.40 ± 2.2	1.27	-2.79 ± 8.23	0.68
Cape Point	SAWS	-10.23 ± 3.84	5.33	-3.35 ± 3.56	1.88	+6.62 ± 5.77	2.30
Casey Station	CSIRO	-6.26 ± 5.28	2.37	-2.25 ± 1.83	2.45	-0.98 ± 5.63	0.35
Halley Bay	NOAA/ESRL	-1.10 ± 4.61	0.47	-1.98 ± 1.76	2.26	-0.68 ± 5.34	0.25
Hegyhatsal	NOAA/ESRL	-52.26 ± 31.63	3.30	+2.12 ± 6.46	0.66	-52.73 ± 6.90	15.28
Heimaey	NOAA/ESRL	-13.54 ± 16.28	1.66	-1.51 ± 2.45	1.23	-17.68 ± 10.17	3.48
Izña (Tenerife)	NOAA/ESRL	-4.89 ± 10.04	0.97	+0.02 ± 3.29	0.01	-13.02 ± 5.20	5.01
Key Biscayne	NOAA/ESRL	+5.03 ± 16.49	0.61	+3.40 ± 6.94	0.98	-15.14 ± 6.50	4.66
Mace Head	AGAGE	-9.059 ± 15.53	1.17	-2.51 ± 5.41	0.93	-22.39 ± 8.26	5.42
Mace Head	NOAA/ESRL	-18.81 ± 14.63	2.57	-2.51 ± 5.41	0.93	-22.39 ± 8.26	5.42
Macquarie Island	CSIRO	-5.35 ± 3.55	3.01	-2.38 ± 1.50	3.18	-1.15 ± 5.50	0.42
Mahe Island	NOAA/ESRL	+5.89 ± 10.85	1.08	-3.40 ± 3.43	1.98	-1.83 ± 4.96	0.74
Mauna Loa	NOAA/ESRL	-8.11 ± 11.40	1.42	-1.40 ± 2.45	1.14	-5.49 ± 4.89	2.25
Mt. Waiiguan	NOAA/ESRL, CMA	-3.18 ± 24.61	0.26	-4.64 ± 11.22	0.83	-1.68 ± 12.61	0.27

Title Page	
Abstract	Introduction
Conclusions	References
Tables	Figures
◀	▶
◀	▶
Back	Close
Full Screen / Esc	
Printer-friendly Version	
Interactive Discussion	



Model simulated trend of surface carbon monoxide

J. Yoon and A. Pozzer

Table 4. Continued.

Station	Contributor	WDCGG-archived surface CO $\dot{\phi} \pm 2\sigma_{\dot{\phi}}$ [ppbvdecade $^{-1}$]	$ \dot{\phi}/\sigma_{\dot{\phi}} $ [unitless]	EMAC-simulated surface CO on CE scenario $\dot{\phi} \pm 2\sigma_{\dot{\phi}}$ [ppbvdecade $^{-1}$]	$ \dot{\phi}/\sigma_{\dot{\phi}} $ [unitless]	EMAC-simulated surface CO on RG scenario $\dot{\phi} \pm 2\sigma_{\dot{\phi}}$ [ppbvdecade $^{-1}$]	$ \dot{\phi}/\sigma_{\dot{\phi}} $ [unitless]
Niwot Ridge (T-van)	NOAA/ESRL	-11.42 ± 11.89	1.92	-8.85 ± 8.33	2.12	-67.85 ± 9.97	13.61
Park Falls	NOAA/ESRL	-17.68 ± 15.16	2.33	-0.03 ± 8.77	0.01	-58.70 ± 11.67	10.06
Palmer Station	NOAA/ESRL	-0.05 ± 5.30	0.02	-2.21 ± 1.76	2.51	-0.94 ± 5.59	0.34
Payerne	Empa	-52.76 ± 22.21	4.75	+6.73 ± 9.53	1.41	-55.53 ± 7.60	14.61
Point Arena	NOAA/ESRL	-11.30 ± 14.28	1.58	-0.84 ± 13.39	0.13	-36.40 ± 19.73	3.69
Hagede Point	NOAA/ESRL	-0.84 ± 6.08	0.28	-0.35 ± 1.87	0.37	-3.24 ± 2.19	2.96
Rigi	Empa	-16.06 ± 19.39	1.66	-0.54 ± 11.34	0.10	-77.92 ± 9.02	17.27
Ryori	JMA	-8.26 ± 9.40	1.76	-3.54 ± 5.85	1.21	-17.47 ± 11.15	3.13
Sand Island	NOAA/ESRL	-8.65 ± 15.33	1.13	-2.21 ± 3.46	1.28	-7.31 ± 6.60	2.22
Sede Boker	NOAA/ESRL	-16.49 ± 15.68	2.10	+0.23 ± 6.14	0.08	+2.91 ± 7.11	0.82
South Pole	CSIRO	-6.65 ± 3.77	3.53	-2.04 ± 1.73	2.36	-0.74 ± 5.28	0.28
South Pole	NOAA/ESRL	+0.96 ± 5.38	0.36	-2.04 ± 1.73	2.36	-0.74 ± 5.28	0.28
Syowa Station	NOAA/ESRL	+0.08 ± 4.88	0.03	-2.21 ± 1.67	2.65	-0.91 ± 5.20	0.35
Tae-ahn Peninsula	NOAA/ESRL	+18.32 ± 36.25	1.01	+2.18 ± 16.26	0.27	-1.37 ± 20.77	0.13
Tudor Hill	NOAA/ESRL	-9.45 ± 12.53	1.51	+3.36 ± 4.34	1.55	-13.51 ± 5.81	4.65
Tutuila (Cape Matatula)	NOAA/ESRL	+2.39 ± 4.57	1.04	-3.15 ± 1.29	4.89	-2.93 ± 2.60	2.25
Ulaan Uul	NOAA/ESRL	-22.21 ± 32.76	1.36	-0.55 ± 6.57	0.17	-15.30 ± 22.40	1.37
Wendover	NOAA/ESRL	-11.05 ± 12.24	1.81	-5.43 ± 4.83	2.25	-27.26 ± 7.27	7.51
Yonagunijima	JMA	-8.50 ± 13.84	1.23	-4.97 ± 6.52	1.52	-6.73 ± 8.61	1.56
Zeppelinfjellet (Ny-Alesund)	NOAA/ESRL	-15.61 ± 19.50	1.60	-0.21 ± 2.33	0.18	-15.90 ± 10.49	3.03

Title Page

Abstract

Introduction

Conclusions

References

Tables

Figures

◀

▶

◀

▶

Back

Close

Full Screen / Esc

Printer-friendly Version

Interactive Discussion



**Model simulated
trend of surface
carbon monoxide**

J. Yoon and A. Pozzer

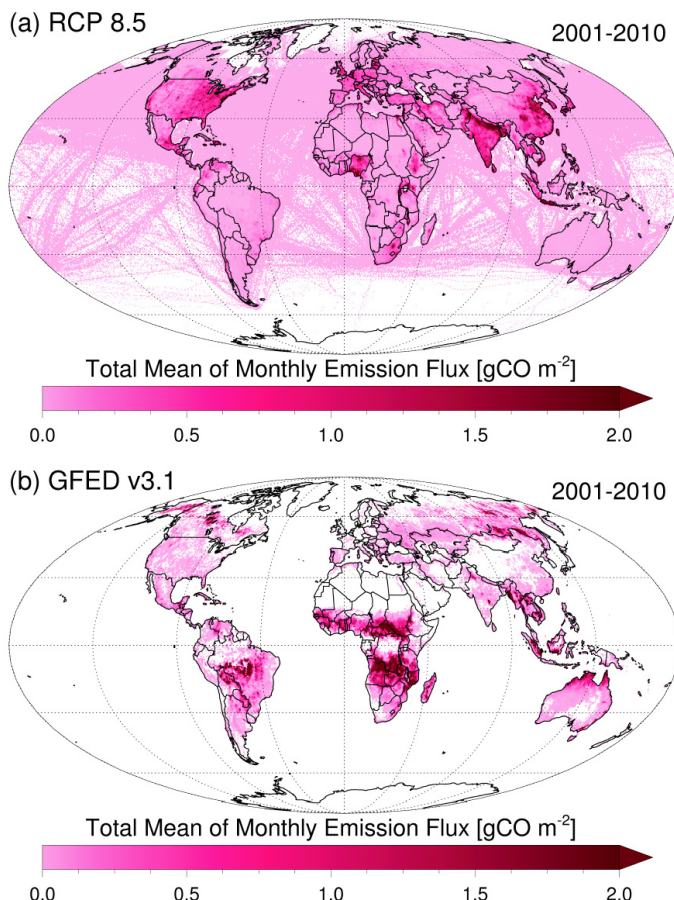


Fig. 1. Global distributions of the total mean of monthly CO emission fluxes of (a) RCP 8.5 and (b) GFED v3.1 from 2001 and 2010.

**Model simulated
trend of surface
carbon monoxide**

J. Yoon and A. Pozzer

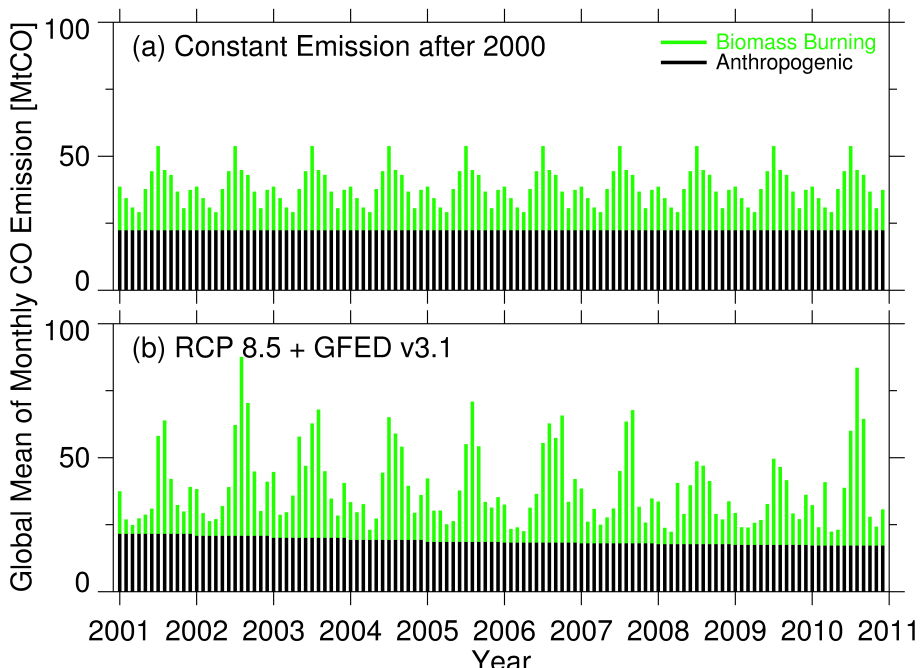


Fig. 2. Time series of the global mean of monthly CO emissions, **(a)** a constant emission of RCP 8.5 and GFED v3.1 after 2000 and **(b)** the combination of RCP 8.5 and GFED v3.1.

- [Title Page](#)
- [Abstract](#) [Introduction](#)
- [Conclusions](#) [References](#)
- [Tables](#) [Figures](#)
- [◀](#) [▶](#)
- [◀](#) [▶](#)
- [Back](#) [Close](#)
- [Full Screen / Esc](#)
- [Printer-friendly Version](#)
- [Interactive Discussion](#)

**Model simulated
trend of surface
carbon monoxide**

J. Yoon and A. Pozzer

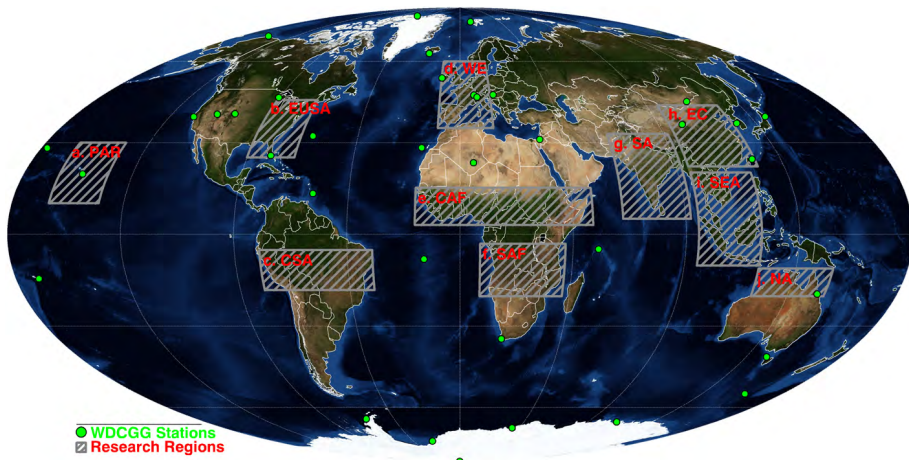


Fig. 3. Research region domains and geolocations of WDCGG stations listed on Tables 1 and 2, respectively.

[Title Page](#)[Abstract](#)[Introduction](#)[Conclusions](#)[References](#)[Tables](#)[Figures](#)[|◀](#)[▶|](#)[Back](#)[Close](#)[Full Screen / Esc](#)[Printer-friendly Version](#)[Interactive Discussion](#)

**Model simulated
trend of surface
carbon monoxide**

J. Yoon and A. Pozzer

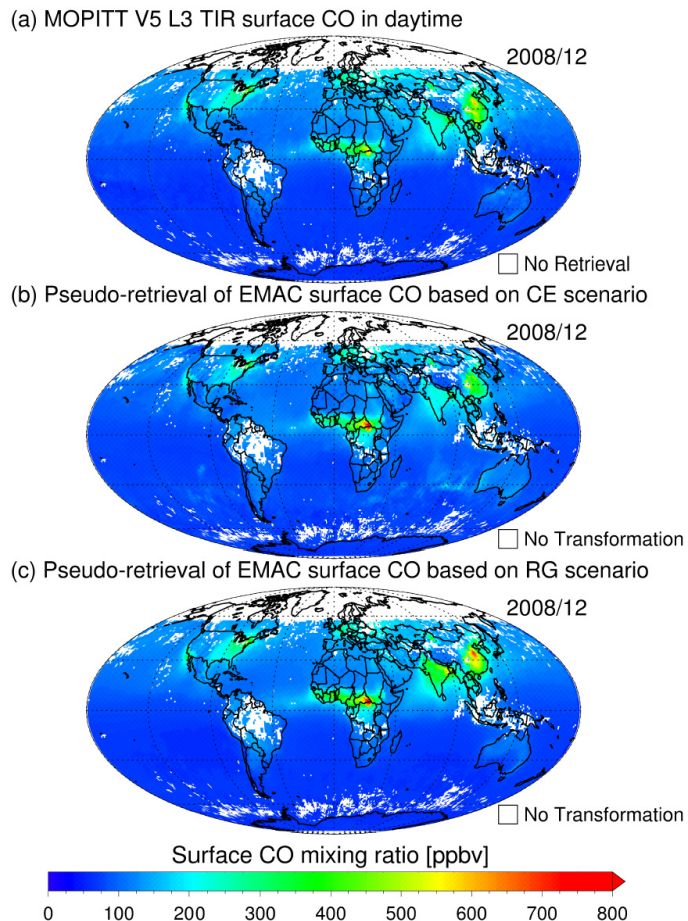


Fig. 4. Global distributions of (a) the MOPITT-retrieved surface CO and pseudo-retrievals of EMAC-simulated surface CO based on (b) CE and (c) RG scenarios on December 2008.

[Title Page](#)[Abstract](#)[Introduction](#)[Conclusions](#)[References](#)[Tables](#)[Figures](#)[|◀](#)[▶|](#)[Back](#)[Close](#)[Full Screen / Esc](#)[Printer-friendly Version](#)[Interactive Discussion](#)

Model simulated trend of surface carbon monoxide

J. Yoon and A. Pozzer

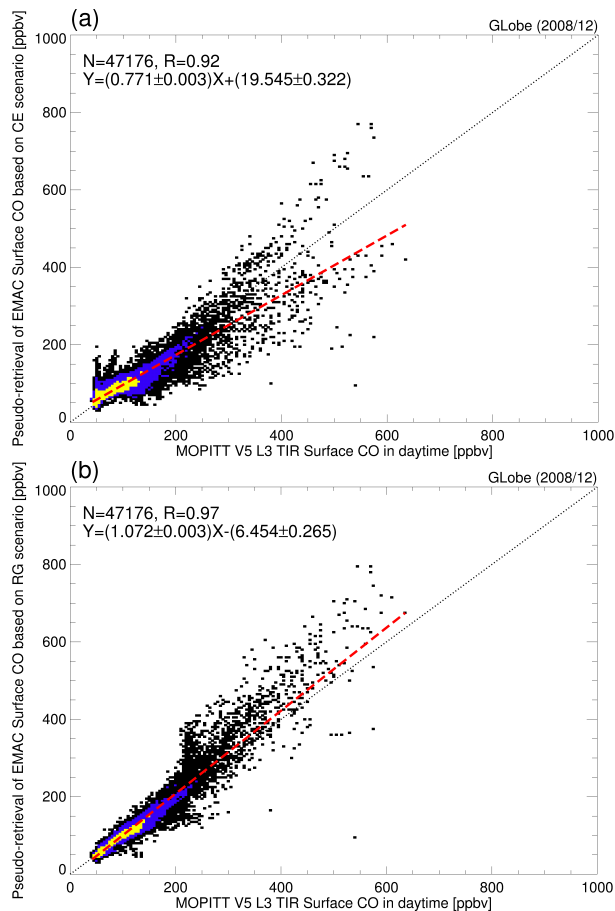


Fig. 5. Spatial comparisons of global MOPITT-retrieved surface CO with the pseudo-retrievals of EMAC simulations based on **(a)** CE and **(b)** RG scenarios on December 2008.

Model simulated trend of surface carbon monoxide

J. Yoon and A. Pozzer

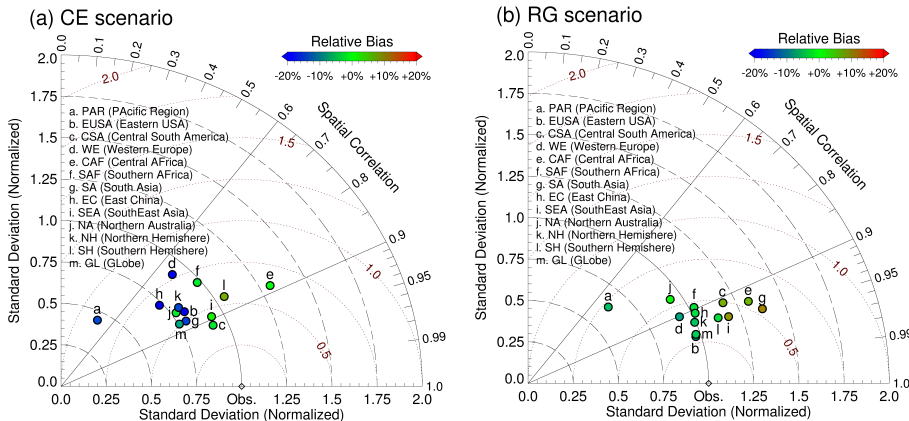


Fig. 6. Spatial pattern analyses of the pseudo-retrievals of EMAC simulations based on **(a)** CE and **(b)** RG scenarios against MOPITT-retrieved surface CO for selected region domains listed on Table 1. Detailed statistical quantities are summarized in Table 3.

- [Title Page](#)
- [Abstract](#) [Introduction](#)
- [Conclusions](#) [References](#)
- [Tables](#) [Figures](#)
- [◀](#) [▶](#)
- [◀](#) [▶](#)
- [Back](#) [Close](#)
- [Full Screen / Esc](#)
- [Printer-friendly Version](#)
- [Interactive Discussion](#)

Model simulated trend of surface carbon monoxide

J. Yoon and A. Pozzer

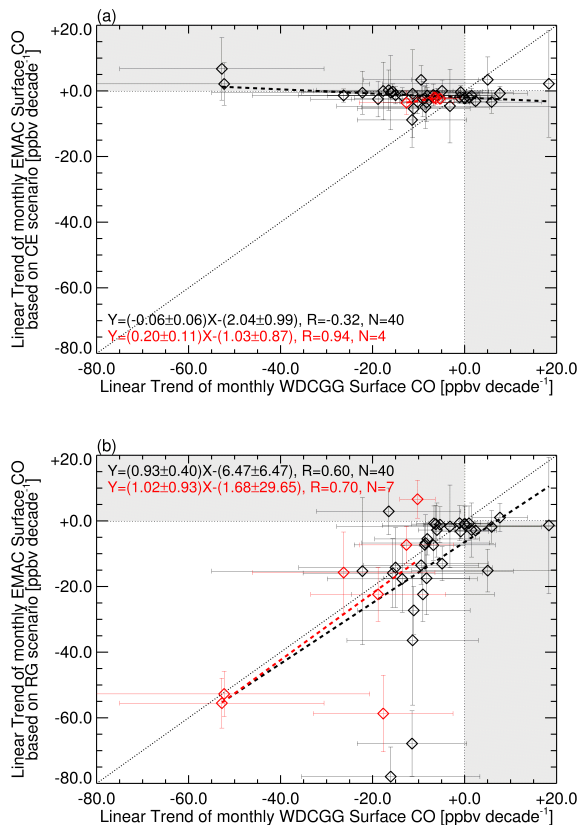


Fig. 7. Comparisons of the trends of monthly EMAC-simulated surface CO based on **(a)** CE and **(b)** RG scenarios against the trend of monthly WDCGG-archived surface CO with $\pm 2\sigma$ errors for selected WDCGG stations listed on Table 2. Black and red fonts indicate the results between all available trends and between only significant trends, respectively. Detailed values are summarized in Table 4.

Model simulated trend of surface carbon monoxide

J. Yoon and A. Pozzer

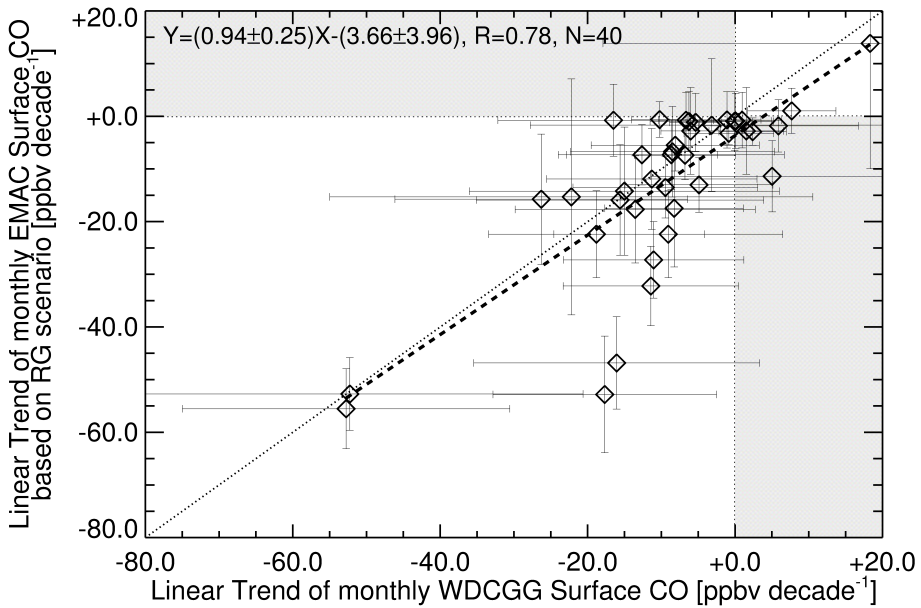


Fig. 8. As in Fig. 7b, but the trends of monthly EMAC-simulated surface CO from a model grid-box to the upwind direction at the stations (i.e. Cape Point, Key Biscayne, Niwot Ridge, Park Falls, Point Arena, Rigi, Sede Boker, and Tae-ahn Peninsula).

Title Page	Abstract	Introduction
Conclusions	References	
Tables	Figures	
◀	▶	
◀	▶	
Back	Close	
Full Screen / Esc		
Printer-friendly Version		
Interactive Discussion		

**Model simulated
trend of surface
carbon monoxide**

J. Yoon and A. Pozzer

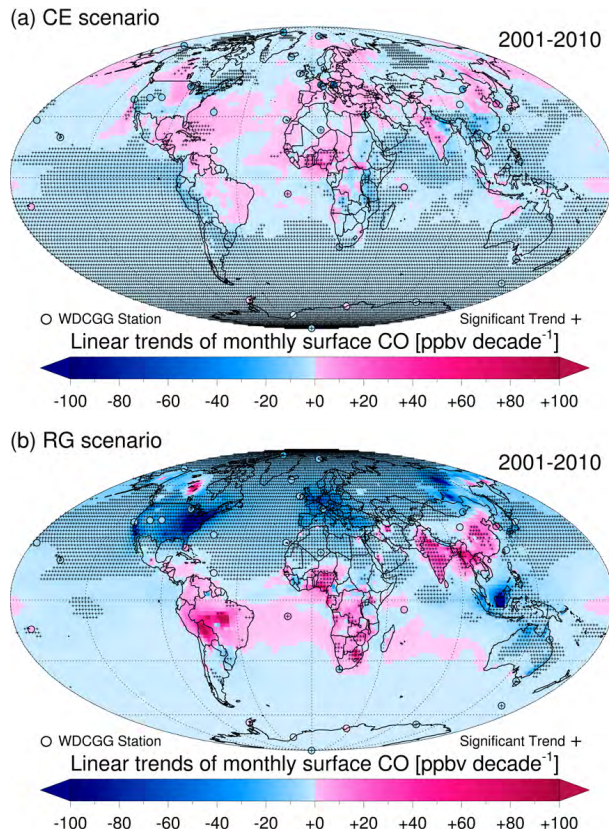


Fig. 9. Global trend estimates of monthly WDCGG-archived and EMAC-simulated surface CO based on (a) CE and (b) RG scenarios from 2001 to 2010. The significant trends are shown as a plus symbol (+).

[Title Page](#)[Abstract](#)[Introduction](#)[Conclusions](#)[References](#)[Tables](#)[Figures](#)[|◀](#)[▶|](#)[◀](#)[▶](#)[Back](#)[Close](#)[Full Screen / Esc](#)[Printer-friendly Version](#)[Interactive Discussion](#)

Model simulated trend of surface carbon monoxide

J. Yoon and A. Pozzer

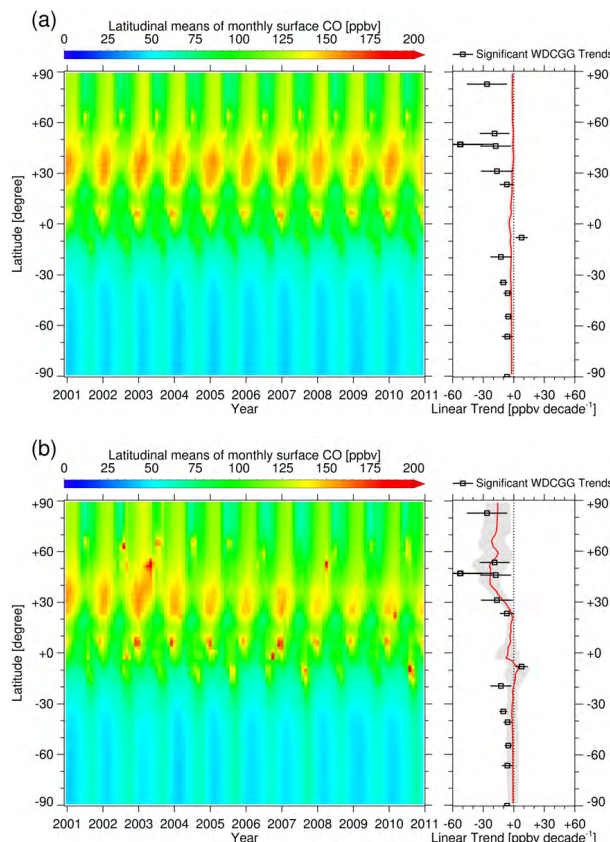


Fig. 10. Latitudinal means and trend estimates of monthly EMAC-simulated surface CO based on **(a)** CE and **(b)** RG scenarios from 2001 to 2010. The significant trends of WDCGG-archived surface CO at a 95 % confidence level are over-plotted to compare with the EMAC latitudinal trends.

Model simulated trend of surface carbon monoxide

J. Yoon and A. Pozzer

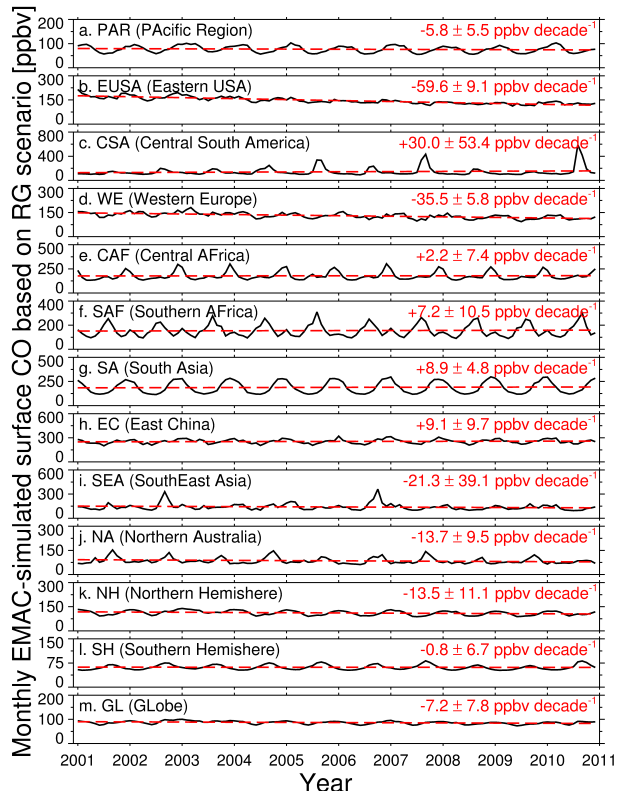


Fig. 11. Regional and global trend estimates of monthly EMAC-simulated surface CO based on RG scenario with $\pm 2\sigma$ errors from 2001 to 2010.

Model simulated trend of surface carbon monoxide

J. Yoon and A. Pozzer

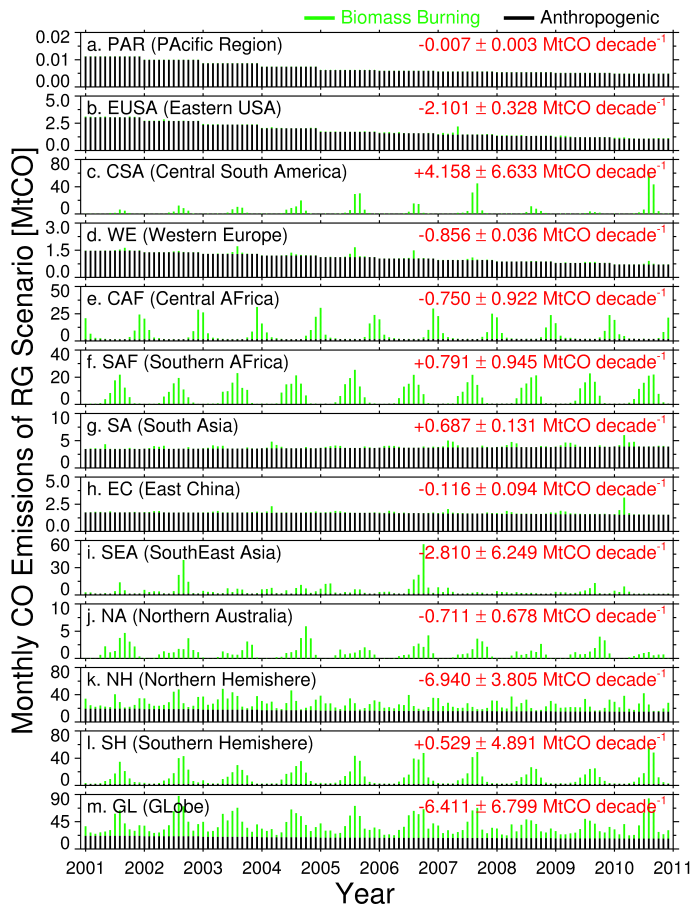


Fig. 12. As in Fig. 11, but ones of monthly RG CO emissions.

Model simulated trend of surface carbon monoxide

J. Yoon and A. Pozzer

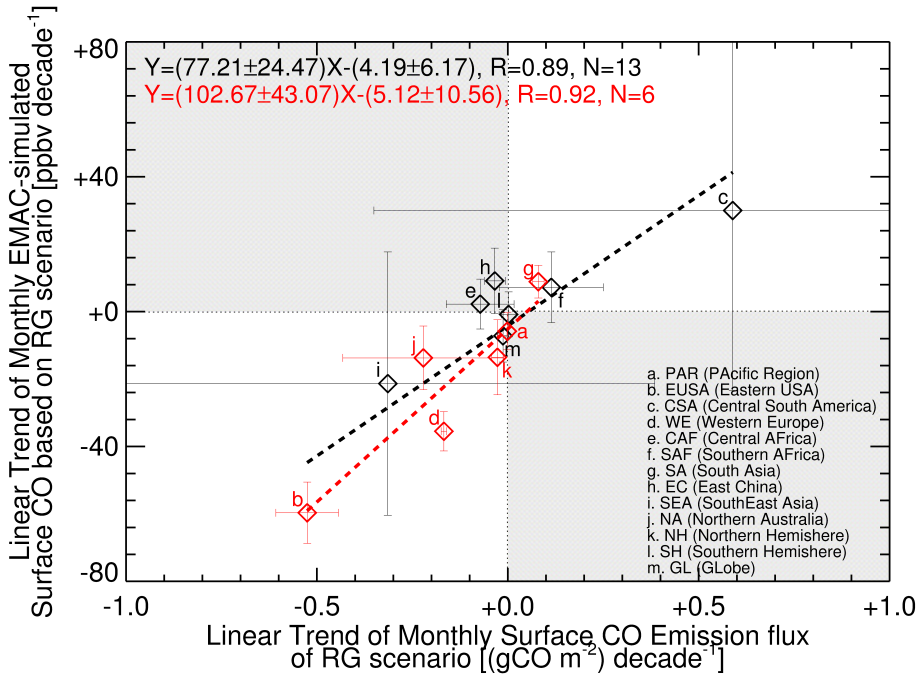


Fig. 13. Comparisons of the trends of monthly RG CO emission flux against the trend of monthly EMAC-simulated surface CO with $\pm 2\sigma$ errors for the selected regions listed on Table 1. Black and red fonts indicate the results between all available trends and between only significant trends, respectively.



Model simulated trend of surface carbon monoxide

J. Yoon and A. Pozzer

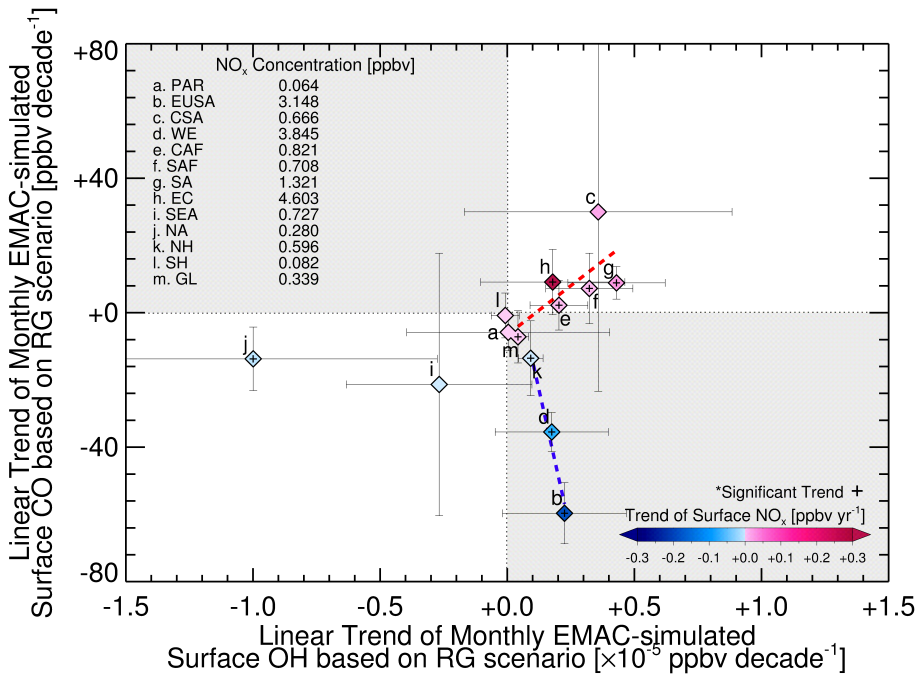


Fig. 14. As in Fig. 13, but trends of monthly EMAC-simulated surface OH with surface NO_x (nitric oxide and nitrogen dioxide) concentration and trend for the selected regions listed on Table 1. The significant trends in surface NO_x are shown as a plus symbol.

[Title Page](#)

[Abstract](#)

[Introduction](#)

[Conclusions](#)

[References](#)

[Tables](#)

[Figures](#)

[|◀](#)

[▶|](#)

[◀](#)

[▶](#)

[Back](#)

[Close](#)

[Full Screen / Esc](#)

[Printer-friendly Version](#)

[Interactive Discussion](#)